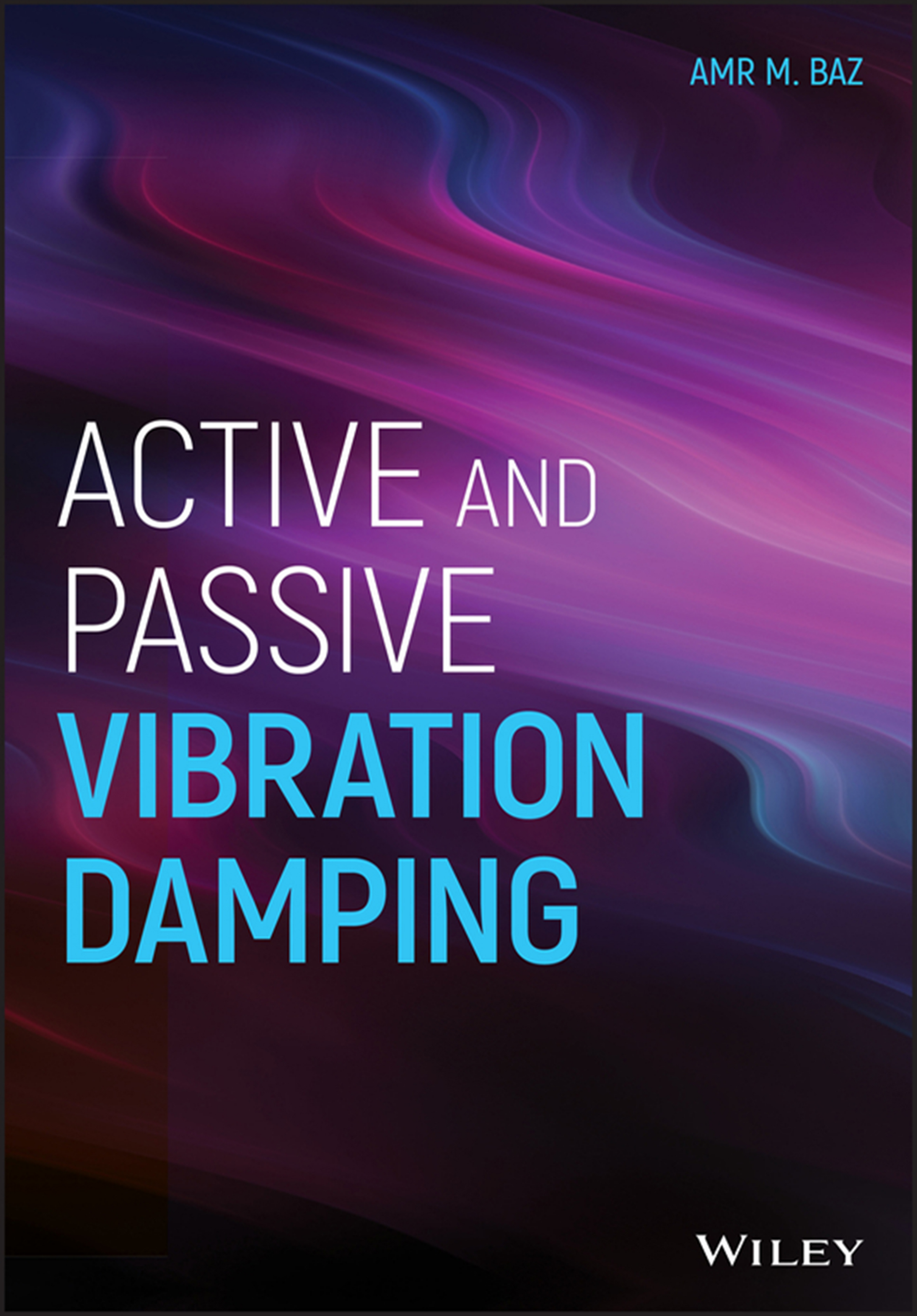

AMR M. BAZ

ACTIVE AND PASSIVE VIBRATION DAMPING

WILEY

Active and Passive Vibration Damping

Active and Passive Vibration Damping

Amr M. Baz
University of Maryland, USA

WILEY

This edition first published 2019
© 2019 John Wiley & Sons Ltd

All rights reserved. No part of this publication may be reproduced, stored in a retrieval system, or transmitted, in any form or by any means, electronic, mechanical, photocopying, recording or otherwise, except as permitted by law. Advice on how to obtain permission to reuse material from this title is available at http://www.wiley.com/go/permissions.

The right of Amr M. Baz to be identified as the author of this work has been asserted in accordance with law.

Registered Offices
John Wiley & Sons, Inc., 111 River Street, Hoboken, NJ 07030, USA
John Wiley & Sons Ltd, The Atrium, Southern Gate, Chichester, West Sussex, PO19 8SQ, UK

Editorial Office
The Atrium, Southern Gate, Chichester, West Sussex, PO19 8SQ, UK

For details of our global editorial offices, customer services, and more information about Wiley products visit us at www.wiley.com.

Wiley also publishes its books in a variety of electronic formats and by print-on-demand. Some content that appears in standard print versions of this book may not be available in other formats.

Limit of Liability/Disclaimer of Warranty
While the publisher and authors have used their best efforts in preparing this work, they make no representations or warranties with respect to the accuracy or completeness of the contents of this work and specifically disclaim all warranties, including without limitation any implied warranties of merchantability or fitness for a particular purpose. No warranty may be created or extended by sales representatives, written sales materials or promotional statements for this work. The fact that an organization, website, or product is referred to in this work as a citation and/or potential source of further information does not mean that the publisher and authors endorse the information or services the organization, website, or product may provide or recommendations it may make. This work is sold with the understanding that the publisher is not engaged in rendering professional services. The advice and strategies contained herein may not be suitable for your situation. You should consult with a specialist where appropriate. Further, readers should be aware that websites listed in this work may have changed or disappeared between when this work was written and when it is read. Neither the publisher nor authors shall be liable for any loss of profit or any other commercial damages, including but not limited to special, incidental, consequential, or other damages.

MATLAB® is a trademark of The MathWorks, Inc. and is used with permission. The MathWorks does not warrant the accuracy of the text or exercises in this book. This work's use or discussion of MATLAB® software or related products does not constitute endorsement or sponsorship by The MathWorks of a particular pedagogical approach or particular use of the MATLAB® software.

Library of Congress Cataloging-in-Publication Data

Names: Baz, Amr Mahmoud Sabry, 1945– author.
Title: Active and passive vibration damping / Amr M. Baz.
Description: Hoboken, NJ, USA : John Wiley & Sons, Inc., [2019] | Includes bibliographical references and index. |
Identifiers: LCCN 2018027360 (print) | LCCN 2018030715 (ebook) | ISBN 9781118537589 (Adobe PDF) | ISBN 9781118537602 (ePub) | ISBN 9781118481929 (hardcover)
Subjects: LCSH: Damping (Mechanics) | Vibration.
Classification: LCC TA355 (ebook) | LCC TA355 .B368 2018 (print) | DDC 620.3/7–dc23
LC record available at https://lccn.loc.gov/2018027360

Cover Design: Wiley
Cover Image: © oxygen / Moment/ Getty Images

Set in 10/12pt Warnock by SPi Global, Pondicherry, India

Printed and bound by CPI Group (UK) Ltd, Croydon, CR0 4YY

10 9 8 7 6 5 4 3 2 1

To the memory of my father and sister.

Contents

Preface *xvii*
List of Symbols *xxi*
Abbreviations *xxxi*

Part I Fundamentals of Viscoelastic Damping *1*

1 Vibration Damping *3*
- 1.1 Overview *3*
- 1.2 Passive, Active, and Hybrid Vibration Control *3*
  - 1.2.1 Passive Damping *3*
    - 1.2.1.1 Free and Constrained Damping Layers *3*
    - 1.2.1.2 Shunted Piezoelectric Treatments *4*
    - 1.2.1.3 Damping Layers with Shunted Piezoelectric Treatments *5*
    - 1.2.1.4 Magnetic Constrained Layer Damping (MCLD) *5*
    - 1.2.1.5 Damping with Shape Memory Fibers *6*
  - 1.2.2 Active Damping *6*
  - 1.2.3 Hybrid Damping *7*
    - 1.2.3.1 Active Constrained Layer Damping (ACLD) *7*
    - 1.2.3.2 Active Piezoelectric Damping Composites (APDC) *7*
    - 1.2.3.3 Electromagnetic Damping Composites (EMDC) *8*
    - 1.2.3.4 Active Shunted Piezoelectric Networks *8*
- 1.3 Summary *9*
  - References *9*

2 Viscoelastic Damping *11*
- 2.1 Introduction *11*
- 2.2 Classical Models of Viscoelastic Materials *11*
  - 2.2.1 Characteristics in the Time Domain *11*
  - 2.2.2 Basics for Time Domain Analysis *12*
  - 2.2.3 Detailed Time Response of Maxwell and Kelvin–Voigt Models *14*
  - 2.2.4 Detailed Time Response of the Poynting–Thomson Model *17*
- 2.3 Creep Compliance and Relaxation Modulus *20*
  - 2.3.1 Direct Laplace Transformation Approach *22*
  - 2.3.2 Approach of Simultaneous Solution of a Linear Set of Equilibrium, Kinematic, and Constitutive Equations *23*

2.4 Characteristics of the VEM in the Frequency Domain *25*
2.5 Hysteresis and Energy Dissipation Characteristics of Viscoelastic Materials *27*
  2.5.1 Hysteresis Characteristics *27*
  2.5.2 Energy Dissipation *28*
  2.5.3 Loss Factor *28*
    2.5.3.1 Relationship Between Dissipation and Stored Elastic Energies *28*
    2.5.3.2 Relationship Between Different Strains *29*
  2.5.4 Storage Modulus *29*
2.6 Fractional Derivative Models of Viscoelastic Materials *32*
  2.6.1 Basic Building Block of Fractional Derivative Models *32*
  2.6.2 Basic Fractional Derivative Models *33*
  2.6.3 Other Common Fractional Derivative Models *36*
2.7 Viscoelastic Versus Other Types of Damping Mechanisms *38*
2.8 Summary *40*
References *40*

3 Characterization of the Properties of Viscoelastic Materials *57*
3.1 Introduction *57*
3.2 Typical Behavior of Viscoelastic Materials *57*
3.3 Frequency Domain Measurement Techniques of the Dynamic Properties of Viscoelastic Material *59*
  3.3.1 Dynamic, Mechanical, and Thermal Analyzer *60*
  3.3.2 Oberst Test Beam Method *64*
    3.3.2.1 Set-Up and Beam Configurations *64*
    3.3.2.2 Parameter Extraction *66*
3.4 Master Curves of Viscoelastic Materials *68*
  3.4.1 The Principle of Temperature-Frequency Superposition *68*
  3.4.2 The Use of the Master Curves *71*
  3.4.3 The Constant Temperature Lines *71*
3.5 Time-Domain Measurement Techniques of the Dynamic Properties of Viscoelastic Materials *72*
  3.5.1 Creep and Relaxation Measurement Methods *73*
    3.5.1.1 Testing Equipment *73*
    3.5.1.2 Typical Creep and Relaxation Behavior *74*
    3.5.1.3 Time-Temperature Superposition *76*
    3.5.1.4 Boltzmann Superposition Principle *78*
    3.5.1.5 Relationship Between the Relaxation Modulus and Complex Modulus *80*
    3.5.1.6 Relationship Between the Creep Compliance and Complex Compliance *81*
    3.5.1.7 Relationship Between the Creep Compliance and Relaxation Modulus *83*
    3.5.1.8 Alternative Relationship Between the Creep Compliance and Complex Compliance *83*
    3.5.1.9 Alternative Relationship Between the Relaxation Modulus and Complex Modulus *84*

- 3.5.1.10 Summary of the Basic Interconversion Relationship *85*
- 3.5.1.11 Practical Issues in Implementation of Interconversion Relationships *86*
- 3.5.2 Split Hopkinson Pressure Bar Method *94*
  - 3.5.2.1 Overview *94*
  - 3.5.2.2 Theory of 1D SHPB *95*
  - 3.5.2.3 Complex Modulus of a VEM from SHPB Measurements *98*
- 3.5.3 Wave Propagation Method *105*
- 3.5.4 Ultrasonic Wave Propagation Method *109*
  - 3.5.4.1 Overview *109*
  - 3.5.4.2 Theory *109*
  - 3.5.4.3 Measurement of the Phase Velocity and Attenuation Factor *111*
  - 3.5.4.4 Typical Attenuation Factors *113*
- 3.6 Summary *115*
- References *116*

4 Viscoelastic Materials *127*

- 4.1 Introduction *127*
- 4.2 Golla–Hughes–McTavish (GHM) Model *127*
  - 4.2.1 Motivation of the *GHM* Model *128*
  - 4.2.2 Computation of the Parameters of the *GHM* Mini-Oscillators *132*
  - 4.2.3 On the Structure of the GHM Model *135*
    - 4.2.3.1 Other Forms of GHM Structures *135*
    - 4.2.3.2 Relaxation Modulus of the GHM Model *135*
  - 4.2.4 Structural Finite Element Models of Rods Treated with VEM *137*
    - 4.2.4.1 Unconstrained Layer Damping *138*
    - 4.2.4.2 Constrained Layer Damping *142*
- 4.3 Structural Finite Element Models of Beams Treated with VEM *150*
  - 4.3.1 Degrees of Freedom *150*
  - 4.3.2 Basic Kinematic Relationships *151*
  - 4.3.3 Stiffness and Mass Matrices of the Beam/VEM Element *152*
  - 4.3.4 Equations of Motion of the Beam/VEM Element *153*
- 4.4 Generalized Maxwell Model (GMM) *155*
  - 4.4.1 Overview *155*
  - 4.4.2 Internal Variable Representation of the GMM *157*
    - 4.4.2.1 Single-DOF System *157*
    - 4.4.2.2 Multi-Degree of Freedom System *158*
    - 4.4.2.3 Condensation of the Internal Degrees of Freedom *159*
    - 4.4.2.4 Direct Solution of Coupled Structural and Internal Degrees of Freedom *160*
- 4.5 Augmenting Thermodynamic Field (ATF) Model *163*
  - 4.5.1 Overview *163*
  - 4.5.2 Equivalent Damping Ratio of the *ATF* Model *164*
  - 4.5.3 Multi-degree of Freedom ATF Model *165*
  - 4.5.4 Integration with a Finite Element Model *165*
- 4.6 Fractional Derivative (FD) Models *167*
  - 4.6.1 Overview *167*

- 4.6.2 Internal Degrees of Freedom of Fractional Derivative Models *169*
- 4.6.3 Grunwald Approximation of Fractional Derivative *169*
- 4.6.4 Integration Fractional Derivative Approximation with Finite Element *170*
  - 4.6.4.1 Viscoelastic Rod *170*
  - 4.6.4.2 Beam with Passive Constrained Layer Damping (PCLD) Treatment *172*

4.7 Finite Element Modeling of Plates Treated with Passive Constrained Layer Damping *176*

- 4.7.1 Overview *176*
- 4.7.2 The Stress and Strain Characteristics *178*
  - 4.7.2.1 The Plate and the Constraining Layers *178*
  - 4.7.2.2 The VEM Layer *179*
- 4.7.3 The Potential and Kinetic Energies *179*
- 4.7.4 The Shape Functions *179*
- 4.7.5 The Stiffness Matrices *181*
- 4.7.6 The Mass Matrices *181*
- 4.7.7 The Element and Overall Equations of Motion *182*

4.8 Finite Element Modeling of Shells Treated with Passive Constrained Layer Damping *185*

- 4.8.1 Overview *185*
- 4.8.2 Stress–Strain Relationships *186*
  - 4.8.2.1 Shell and Constraining Layer *186*
  - 4.8.2.2 Viscoelastic Layer *187*
- 4.8.3 Kinetic and Potential Energies *189*
- 4.8.4 The Shape Functions *189*
- 4.8.5 The Stiffness Matrices *189*
- 4.8.6 The Mass Matrices *190*
- 4.8.7 The Element and Overall Equations of Motion *191*

4.9 Summary *192*

References *196*

5 Finite Element Modeling of Viscoelastic Damping by Modal Strain Energy Method *205*

5.1 Introduction *205*

5.2 Modal Strain Energy (MSE) Method *205*

5.3 Modified Modal Strain Energy (MSE) Methods *210*

- 5.3.1 Weighted Stiffness Matrix Method (WSM) *210*
- 5.3.2 Weighted Storage Modulus Method (WSTM) *211*
- 5.3.3 Improved Reduction System Method (IRS) *211*
- 5.3.4 Low Frequency Approximation Method (LFA) *213*

5.4 Summary of Modal Strain Energy Methods *215*

5.5 Modal Strain Energy as a Metric for Design of Damping Treatments *215*

5.6 Perforated Damping Treatments *220*

- 5.6.1 Overview *220*
- 5.6.2 Finite Element Modeling *222*
  - 5.6.2.1 Element Energies *224*

        - 5.6.2.2 Topology Optimization of Unconstrained Layer Damping *227*
        - 5.6.2.3 Sensitivity Analysis *228*
- 5.7 Summary *234*
- References *234*

6 Energy Dissipation in Damping Treatments *243*

- 6.1 Introduction *243*
- 6.2 Passive Damping Treatments of Rods *243*
    - 6.2.1 Passive Constrained Layer Damping *243*
        - 6.2.1.1 Equation of Motion *243*
        - 6.2.1.2 Energy Dissipation *247*
    - 6.2.2 Passive Unconstrained Layer Damping *248*
- 6.3 Active Constrained Layer Damping Treatments of Rods *251*
    - 6.3.1 Equation of Motion *251*
    - 6.3.2 Boundary Control Strategy *253*
    - 6.3.3 Energy Dissipation *254*
- 6.4 Passive Constrained Layer Damping Treatments of Beams *257*
    - 6.4.1 Basic Equations of Damped Beams *257*
    - 6.4.2 Bending Energy of Beams *258*
    - 6.4.3 Energy Dissipated in Beams with Passive Constrained Layer Damping *258*
- 6.5 Active Constrained Layer Damping Treatments of Beams *264*
- 6.6 Passive and Active Constrained Layer Damping Treatments of Plates *267*
    - 6.6.1 Kinematic Relationships *268*
    - 6.6.2 Energies of the PCLD and ACLD Treatments *269*
        - 6.6.2.1 The Potential Energies *269*
        - 6.6.2.2 The Kinetic Energy *269*
        - 6.6.2.3 Work Done *269*
    - 6.6.3 The Models of the PCLD and ACLD Treatments *270*
    - 6.6.4 Boundary Control of Plates with ACLD Treatments *270*
    - 6.6.5 Energy Dissipation and Loss Factors of Plates with PCLD and ACLD Treatments *271*
- 6.7 Passive and Active Constrained Layer Damping Treatments of Axi-Symmetric Shells *274*
    - 6.7.1 Background *275*
    - 6.7.2 The Concept of the Active Constrained Layer Damping *276*
    - 6.7.3 Variational Modeling of the Shell/ACLD System *276*
        - 6.7.3.1 Main Assumptions of the Model *276*
        - 6.7.3.2 Kinematic Relationships *276*
        - 6.7.3.3 Stress-Strain Relationships *277*
        - 6.7.3.4 Energies of Shell/ACLD System *279*
        - 6.7.3.5 The Model *280*
    - 6.7.4 Boundary Control Strategy *282*
        - 6.7.4.1 Overview *282*
        - 6.7.4.2 Control Strategy *282*
        - 6.7.4.3 Implementation of the Boundary Control Strategy *283*

- 6.7.4.4 Transverse Compliance and Longitudinal Deflection *283*
- 6.7.5 Energy Dissipated in the ACLD Treatment of an Axi-Symmetric Shell *287*
- 6.8 Summary *288*
- References *290*

Part II Advanced Damping Treatments *301*

7 Vibration Damping of Structures Using Active Constrained Layer Damping *303*

- 7.1 Introduction *303*
- 7.2 Motivation for Using Passive and Active Constrained Layer Damping *303*
  - 7.2.1 Base Structure *304*
  - 7.2.2 Structure Treated with Unconstrained Passive Layer Damping *306*
  - 7.2.3 Structure Treated with Constrained Passive Layer Damping *308*
  - 7.2.4 Structure Treated with Active Constrained Passive Layer Damping *311*
- 7.3 Active Constrained Layer Damping for Beams *316*
  - 7.3.1 Introduction *316*
  - 7.3.2 Concept of Active Constrained Layer Damping *316*
  - 7.3.3 Finite Element Modeling of a Beam/ACLD Assembly *318*
    - 7.3.3.1 The Model *319*
    - 7.3.3.2 Equations of Motion *322*
  - 7.3.4 Distributed-Parameter Modeling of a Beam/ACLD Assembly *328*
    - 7.3.4.1 Overview *328*
    - 7.3.4.2 The Energies and Work Done on the Beam/ACLD Assembly *328*
    - 7.3.4.3 The Distributed-Parameter Model *331*
    - 7.3.4.4 Globally Stable Boundary Control Strategy *333*
    - 7.3.4.5 Implementation of the Globally Stable Boundary Control Strategy *333*
    - 7.3.4.6 Response of the Beam/ACLD Assembly *334*
- 7.4 Active Constrained Layer Damping for Plates *336*
  - 7.4.1 Control Forces and Moments Generated by the Active Constraining Layer *337*
    - 7.4.1.1 The In-Plane Piezoelectric Forces *337*
    - 7.4.1.2 The Piezoelectric Moments *338*
    - 7.4.1.3 Piezoelectric Sensor *338*
    - 7.4.1.4 Control Voltage to Piezoelectric Constraining Layer *339*
  - 7.4.2 Equations of Motion *339*
- 7.5 Active Constrained Layer Damping for Shells *344*
  - 7.5.1 Control Forces and Moments Generated by the Active Constraining Layer *344*
  - 7.5.2 Equations of Motion *344*
- 7.6 Summary *348*
- References *351*

8 **Advanced Damping Treatments** 361
8.1 Introduction 361
8.2 Stand-Off Damping Treatments 362
8.2.1 Background of Stand-Off Damping Treatments 362
8.2.2 The Stand-Off Damping Treatments 362
8.2.3 Distributed-Parameter Model of the Stand-Off Layer Damping Treatment 364
8.2.3.1 Kinematic Equations 364
8.2.3.2 Constitutive Equations 365
8.2.4 Distributed Transfer Function Method 369
8.2.5 Finite Element Model 370
8.2.6 Summary 375
8.3 Functionally Graded Damping Treatments 375
8.3.1 Background of Functionally Graded Constrained Layer Damping 375
8.3.2 Concept of Constrained Layer Damping with Functionally Graded Viscoelastic Cores 376
8.3.3 Finite Element Model 377
8.3.3.1 Quasi-Static Model of the Passive Constrained Damping Layer of Plunkett and Lee (1970) 377
8.3.3.2 Dispersion Characteristics of Passive Constrained Damping Layer with Uniform and Functionally Graded Cores 383
8.3.4 Summary 390
8.4 Passive and Active Damping Composite Treatments 390
8.4.1 Passive Composite Damping Treatments 390
8.4.2 Active Composite Damping Treatments 394
8.4.3 Finite Element Modeling of Beam with APDC 396
8.4.3.1 Model and Main Assumptions 396
8.4.3.2 Kinematics 397
8.4.3.3 Degrees of Freedom and Shape Functions 398
8.4.3.4 System Energies 398
8.4.3.5 Equations of Motion 400
8.4.3.6 Control Law 400
8.4.4 Summary 408
8.5 Magnetic Damping Treatments 410
8.5.1 Magnetic Constrained Layer Damping Treatments 410
8.5.2 Analysis of Magnetic Constrained Layer Damping Treatments 412
8.5.2.1 Equation of Motion 412
8.5.2.2 Response of the MCLD Treatment 414
8.5.3 Passive Magnetic Composites 415
8.5.3.1 Concept of Passive Magnetic Composite Treatment 417
8.5.3.2 Finite Element Modeling of Beams with PMC Treatment 417
8.5.4 Summary 430
8.6 Negative Stiffness Composites 430
8.6.1 Motivation to Negative Stiffness Composites 431
8.6.1.1 Sinusoidal Excitation 431

        8.6.1.2 Impact Loading *436*
        8.6.1.3 Magnetic Composite with Negative Stiffness Inclusions *438*
  8.7 Summary *445*
  References *445*

9 Vibration Damping with Shunted Piezoelectric Networks *469*

  9.1 Introduction *469*
  9.2 Shunted Piezoelectric Patches *469*
    9.2.1 Basics of Piezoelectricity *469*
        9.2.1.1 Effect of Electrical Boundary Conditions *471*
        9.2.1.2 Effect of Mechanical Boundary Conditions *471*
    9.2.2 Basics of Shunted Piezo-Networks *472*
        9.2.2.1 Resistive-Shunted Circuit *474*
        9.2.2.2 Resistive and Inductive Shunted Circuit *475*
        9.2.2.3 Resistive, Capacitive, and Inductive Shunted Circuit *477*
    9.2.3 Electronic Synthesis of Inductances and Negative Capacitances *479*
        9.2.3.1 Synthesis of Inductors *479*
        9.2.3.2 Synthesis of Negative Capacitances *480*
    9.2.4 Why Negative Capacitance Is Effective? *480*
    9.2.5 Effectiveness of the Negative Capacitance from a Control System Perspective *482*
    9.2.6 Electrical Analogy of Shunted Piezoelectric Networks *485*
  9.3 Finite Element Modeling of Structures Treated with Shunted Piezo-Networks *487*
    9.3.1 Equivalent Complex Modulus Approach of Shunted Piezo-Networks *487*
    9.3.2 Coupled Electromechanical Field Approach of Shunted Piezo-Networks *491*
  9.4 Active Shunted Piezoelectric Networks *496*
    9.4.1 Basic Configurations *496*
    9.4.2 Dynamic Equations *498*
        9.4.2.1 Short-Circuit Configuration *498*
        9.4.2.2 Open-Circuit Configuration *498*
        9.4.2.3 Resistive-Shunted Configuration *498*
    9.4.3 More on the Resistive Shunting Configuration *498*
    9.4.4 Open-Circuit to Resistive Shunting (OC-RS) Configuration *500*
        9.4.4.1 Dynamic Equations *500*
        9.4.4.2 Switching Between OC and RS Modes *500*
    9.4.5 Energy Dissipation of Different Shunting Configurations *503*
        9.4.5.1 Energy Dissipation with Resistive Shunting *503*
        9.4.5.2 Energy Dissipation with OC-RS Switched Shunting *503*
  9.5 Multi-Mode Vibration Control with Shunted Piezoelectric Networks *504*
    9.5.1 Multi-Mode Shunting Approaches *504*
    9.5.2 Parameters of Behrens et al.'s Multi-Mode Shunting Network *507*
        9.5.2.1 Components of the Current Flowing Branches *507*
        9.5.2.2 Components of the Shunting Branches *507*
  9.6 Summary *510*
  References *511*

10 Vibration Control with Periodic Structures *523*

10.1 Introduction *523*
10.2 Basics of Periodic Structures *524*
  10.2.1 Overview *524*
  10.2.2 Transfer Matrix Method *525*
    10.2.2.1 The Transfer Matrix *525*
    10.2.2.2 Basic Properties of the Transfer Matrix *526*
10.3 Filtering Characteristics of Passive Periodic Structures *533*
  10.3.1 Overview *533*
  10.3.2 Periodic Rods in Longitudinal Vibrations *534*
10.4 Natural Frequencies, Mode Shapes, and Response of Periodic Structures *535*
  10.4.1 Natural Frequencies and Response *535*
  10.4.2 Mode Shapes *539*
10.5 Active Periodic Structures *541*
  10.5.1 Modeling of Active Periodic Structures *543*
  10.5.2 Dynamics of One Cell *543*
    10.5.2.1 Dynamics of the Passive Sub-Cell *543*
    10.5.2.2 Dynamics of the Active Sub-Cell *543*
    10.5.2.3 Dynamics of the Entire Cell *545*
    10.5.2.4 Dynamics of the Entire Periodic Structure *546*
10.6 Localization Characteristics of Passive and Active Aperiodic Structures *549*
  10.6.1 Overview *549*
  10.6.2 Localization Factor *550*
10.7 Periodic Rod with Periodic Shunted Piezoelectric Patches *559*
  10.7.1 Transfer Matrix of a Plain Rod Element *559*
  10.7.2 Transfer Matrix of a Rod/Piezo-Patch Element *560*
  10.7.3 Transfer Matrix of a Unit Cell *561*
10.8 Two-Dimensional Active Periodic Structure *562*
  10.8.1 Dynamics of Unit Cell *562*
  10.8.2 Formulation of Phase Constant Surfaces *566*
  10.8.3 Filtering Characteristics *568*
10.9 Periodic Structures with Internal Resonances *569*
  10.9.1 Dynamics of Conventional Periodic Structure *570*
  10.9.2 Dynamics of Periodic Structure with Internal Resonances *572*
    10.9.2.1 Equivalent Mass. Of the Mass-In-Mass Arrangement *572*
    10.9.2.2 Transfer Matrix of the Mass-In-Mass Arrangement *572*
10.10 Summary *578*
References *578*

11 Nanoparticle Damping Composites *589*

11.1 Introduction *589*
11.2 Nanoparticle-Filled Polymer Composites *590*
  11.2.1 Composites with Unidirectional Inclusions *591*
  11.2.2 Arbitrarily Oriented Inclusion Composites *599*
11.3 Comparisons with Classical Filler Reinforcement Methods *607*

11.4 Applications of Carbon Black/Polymer Composites *614*
  11.4.1 Basic Physical Characteristics *614*
  11.4.2 Modeling of the Piezo-Resistance of CB/Polymer Composites *617*
  11.4.3 The Piezo-Resistivity of CB/Polymer Composites *619*
11.5 CB/Polymer Composite as a Shunting Resistance of Piezoelectric Layers *620*
  11.5.1 Finite Element Model *620*
  11.5.2 Condensed Model of a Unit Cell *624*
11.6 Hybrid Composites with Shunted Piezoelectric Particles *629*
  11.6.1 Composite Description and Assumptions *629*
  11.6.2 Shunted Piezoelectric Inclusions *631*
  11.6.3 Typical Performance Characteristics of Hybrid Composites *631*
11.7 Summary *636*
References *636*

12 Power Flow in Damped Structures *651*
12.1 Introduction *651*
12.2 Vibrational Power *651*
  12.2.1 Basic Definitions *651*
  12.2.2 Relationship to System Energies *652*
  12.2.3 Basic Characteristics of the Power Flow *653*
12.3 Vibrational Power Flow in Beams *656*
12.4 Vibrational Power of Plates *661*
  12.4.1 Basic Equations of Vibrating Plates *661*
  12.4.2 Power Flow and Structural Intensity *662*
  12.4.3 Control of the Power Flow and Structural Intensity *668*
  12.4.4 Power Flow and Structural Intensity for Plates with Passive and Active Constrained Layer Damping Treatments *671*
12.5 Power Flow and Structural Intensity for Shells *679*
12.6 Summary *682*
References *682*

Glossary *699*
Appendix *703*
Index *715*

Preface

This book is intended to present the basic principles and potential applications of passive and active vibration damping technologies. The presentation encompasses a mix between the associated physical fundamentals, governing theories, and optimal design strategies of various configurations of vibration damping treatments. Utilization of smart materials to augment the vibration damping of passive treatments is the common thread that is pursued, in depth, throughout the book.

The focus has been on developing a deeper understanding of the science behind various phenomena that govern the control of structural vibration using appropriate damping techniques. It is my intention, in writing this book, to explain in a simple yet comprehensive manner such scientific basics with particular focus on viscoelastic damping materials and the means for controlling passively and actively their energy dissipation characteristics. The book was developed throughout the years during my teaching of various classes on passive and active vibration and noise control. My research in these areas has enriched my teaching and broadened my understanding of these topics. I have tried to blend simple theory with basic engineering practice to enable the students and practicing engineers to understand the science and apply it with confidence. My guide in this effort has been the saying of Albert Einstein:

> *"Why does this applied science, which saves work and makes life easier, bring us so little happiness? The simple answer runs: Because we have not yet learned to make sensible use of it".*

So, in this book, I have attempted applying the theories to various applications, introducing a wide variety of examples and presenting detailed computer simulations, to make the implementation real and practical.

The book includes 12 chapters divided into two parts. The first part is devoted to outlining the basics of vibration damping and this coverage is divided into six chapters. In the second part, various configurations of advanced vibration damping treatments are presented in four chapters that include applications to different structural systems. Part I starts with an introductory chapter on the field of passive and active vibration damping, followed by Chapter 2 that covers the classical models of viscoelastic damping materials. Chapter 3 presents the important characterization methods of viscoelastic materials both in the frequency and time domains. Advanced modeling techniques of viscoelastic materials are covered in Chapter 4. These methods, which include the Prony series, Gola–Hughes–MacTavish, augmented-temperature field, and fractional derivative methods, are presented to enable modeling the dynamics of structures treated with viscoelastic materials by using the finite element method in both the time and frequency domains. The use of modal strain energy as a metric for predicting the modal loss factor of structures treated with damping materials and for optimal design of damping treatments is discussed in Chapter 5. Estimation of the energy dissipation characteristics of various configurations of passive and active damping treatments is described in Chapter 6 for rods, beams, and plates. Part II presents in Chapter 7 the application of passive and active constrained layer damping treatments to beams, plates, and shells. Chapter 8 deals with modeling of various advanced damping treatments such as: stand-off, functionally graded, active piezoelectric damping composites, and magnetic damping treatments. In Chapters 9 and 10, shunted piezoelectric and periodic treatments are described, respectively, as undamped treatments that behave as conventional damping treatments with potentially tunable characteristics. Chapter 11 presents a wide variety of passive and active nanoparticle damping composites and Chapter 12 looks at the problem of power flow in damped structural systems.

The book has a large number of numerical examples to reinforce the understanding of the theories covered, provide means for exercising the knowledge gained, and emphasize the learning of strategies for the design and application of active and passive vibration damping systems. The examples are supported by a set of MATLAB software modules to enable the designers of vibration damping systems extend the theories presented to various applications.

Each chapter of the book will end with a number of problems that cover the different aspects of theoretical analysis, design, and applications of vibration damping technologies.

In this multi-prong coverage approach, the book is targeted to senior undergraduate students, graduate students, researcher, and practicing engineers who are interested in gaining an in-depth exposure to the field of vibration damping. The presentation and supporting tools associated with the book will enable the readers of having hands-on experience to the analysis, design, optimization, and application of this exciting technology to a wide range of situations.

Writing this book would have been virtually impossible without the tireless support of many students, colleagues, and friends who have enriched my life in many ways. These contributions are apparent throughout the book. In particular, I would like to mention the invaluable inputs and contributions from Professors Wael Akl and Adel Al Sabbagh of Ain Shams University in Cairo, Egypt. Also, thanks are due to Prof. Osama Aldraihem of King Saud University in Saudi Arabia for his collaborations over the years and contributions to Chapter 11 and Prof. Massimo Ruzzene of Georgia Tech for many years of very fruitful collaborations.

Thanks are also due to my colleagues and former students who have pioneered the field of active vibration damping and control including: Dr. Mohamed Raafat, Dr. Soon-Neo Poh of the NSWC Center, Prof. Jeng-Jong Ro at Da-Yeh University in Taiwan, Dr. Tung Huei Chen of the NSWC Center, Dr. Chul-Hue Park at Korea Institute for Robot Industry Advancement (KIRIA), Dr. Charles Kim at NASA-Goddard, Dr. Zheng Gu at Zhejiang Tiatai Liangxin Co. in China, the late Dr. Jaeho Oh, Dr. Adel Omer of the Military Technical College in Cairo, Dr. Ted Shields of Northrop-Grumman, Dr. Peter Herdic of the NRL, Dr. William Laplante the Under Secretary of the Air Force, Prof. Ray Manas of Indian Institute of Technology, Kharagpur, Prof. Mustafa Arafa of the American University in Cairo, Prof. Mohammed Al-Ajami of Kuwait University, Prof.

Mohamed Tawfik of Cairo University, Dr. Mary Leibolt of NSWC, Prof. Mostafa Nouh of SUNY Buffalo, and Prof. John Crassidis of SUNY Buffalo. Thanks are also due to my former students Mr. Atif Chaudry of the US Patent Office and Mr. Giovanni Rosannova of NASA Wallop for their work in passive and active damping.

It is important to note that my work in the area of active vibration damping has been funded primarily by the Army Research Office (ARO) with Dr. Gary Anderson as the technical monitor, the Office of Naval Research (ONR) with Dr. Kam Ng as the technical monitor and by Dr. Turki S. Al-Saud the President of King Abdulaziz City for Science & Technology (KACST), Riyadh. Without their support, trust, and friendship, this work would have not been possible.

Special thanks are also due to the administration of the University of Maryland for providing me with the excellent scholarly environment that enabled me developing my professional career and of course writing this book. Important among those administrators are: former President Dan Mote, now the President of NAE, former Provost William Destler, now the President of RIT, former Provost Nariman Farvardin, now the President of Stevens Institute of Technology, current President of UMD President Wallace Loh, Dean of Engineering Darryll Pines, Prof. Davinder Anand, former Chair of ME Department, Prof. William Fourney, Associate Dean of Engineering, Prof. Avi Bar-Cohen, former Chair of ME Department, and Prof. Balakumar Balachandran the current Chair of the ME Department. Apart from their vast professional impact on me, I sincerely and equally value their friendship and collegiality.

Finally, writing this book has been enjoyable and possible because of the tireless support and sacrifice of my wonderful wife and my two great sons who are my true friends and heroes.

Amr M. Baz
College Park, MD
December 2018

List of Symbols

Symbol	Meaning	Units
a	Dimension of a plate side	m
a	Dilatation or contraction scaling parameter of wavelets Area	— m^2
$\mathbf{A}$	Magnetic potential	Ampere
A_{ATF}	Affinity of the ATF model $(=-\partial f_{ATF}/\partial z)$	N m^{-2} $^{\circ}$K^{-1}
$[A_r^*]$	The correspondence concentration factors of phase, r	—
b	Dimension of a plate side	m
b	Translation parameter of wavelets	s
B	Input state-space matrix	—
$\mathbf{B}$	Magnetic induction	Tesla
$B^{*}{,}_{0}$	Characteristics complex length of passive treatments	m
B_0	The magnetic flux density	Tesla
B_F	The structural susceptance matrix	m (Ns)$^{-1}$
$[B_r^*]$	The correspondence concentration factors of phase, r	—
c	The sound speed	m s^{-1}
c_c	The critical damping coefficient $(=2\sqrt{km})$	Ns m^{-1}
c_d	Damping coefficient of dissipative element	Ns m^{-2}
$[c^*]$	Complex stiffness matrix	N m^{-2}
$[c_r^*]$	Complex stiffness matrix of phase, r	N m^{-2}
C	Measurement state-space matrix Capacitance	— Farad
C_G	Control parameter	—
C^S	Strain-free capacitance	Farad

(*Continued*)

Symbol	Meaning	Units
C^T	Stress-free capacitance	Farad
d_{ij}	Piezo-strain constants in the *i* and *j* directions due to applied electric field in the *k* direction	m V^{-1}
D	Energy dissipated during a full vibration cycle of the viscoelastic material	Nm
D	Denominator of a transfer function	—
D	Nano-particle diameter	m
D_a	Distance between neutral axis of entire sandwiched beam and piezo-actuator	m
D_i	Electrical displacement along the *ith* direction	Coulomb m^{-2}
D_t^*	Complex bending stiffness (= $D_t(1 + i\eta_B)$)	Nm^2
$[D_i]$	Stiffness matrix relating the stress and strain vectors	N m^{-2}
e	Electron charge (=1.60217662 × 10^{-19} Coulombs)	Coulomb
e	Power flow error	Nm s^{-1}
e_{31}	Piezoelectric charge/strain constant (=d_{31}/s_{11}^E)	m^3 (N V) $^{-1}$
E	Young's modulus	N m^{-2}
E_i	Electrical field along the *ith* direction	V m^{-1}
E_n	Total energy ($E_n = PE + KE$)	Nm
$E(t)$	Relaxation modulus	N m^{-2}
E'	Storage modulus	N m^{-2}
E''	Loss modulus	N m^{-2}
E^*	Complex relaxation modulus	N m^{-2}
E_0	Equilibrium modulus	N m^{-2}
E_i	Relaxation strength	N m^{-2}
E_∞	Instantaneous modulus of GMM Un-relaxed or high frequency modulus of elasticity	N m^{-2}
E_iA_i	Longitudinal rigidity	N
E_iI_i	Flexural rigidity	Nm^2
EQ	Product of elastic modulus and first moment of area	Nm^2
f	Frequency	rad s^{-1}, Hz
f_{ATF}	Helmholtz free energy density of the ATF model	N m^{-2}
F	Force	N
F_c	Control force	N
$\mathbf{F_m}$	Magnetic forces	N
$\{F\}$	Force and moment vector	N, NM
g	The shear factor of constrained damping treatments	—
g_{31}	The piezoelectric voltage constant (=d_{31}/ε_{33})	m V^{-1}
G'	Storage modulus in shear	N m^{-2}
G''	Loss modulus in shear	N m^{-2}

Symbol	Meaning	Units
G^*	Complex modulus in shear	$\mathrm{N\,m^{-2}}$
G_F	The structural conductance matrix	$\mathrm{m\ (Ns)^{-1}}$
h	Layer thickness	m
h_P	Plank constant (= 6.626×10^{-34})	$\mathrm{m^2\,kg\,s^{-1}}$
$\mathbf{H}$	Magnetic field	Ampere $\mathrm{m^{-1}}$
i	The "unit" imaginary number = $\sqrt{-1}$	—
I	Area moment of inertia	$\mathrm{m^4}$
I	Performance Index	—
$\mathbf{I}$	Current density	Amperes $\mathrm{m^{-2}}$
$\boldsymbol{I_{x,y}}$	Structural intensity	$\mathrm{Nm\ (sm)^{-1}}$
J^*	Complex creep compliance	$\mathrm{m^2\,N^{-1}}$
J_j	Retardation strength	$\mathrm{N\,m^{-2}}$
$\hat{J}(i\omega)$	Fourier transform of creep compliance	m
J	Performance index	—
$\mathbf{J}$	Jacobian matrix	—
K, k	Stiffness	$\mathrm{N\,m^{-1}}$
$K_{d,p}$	Derivative and proportional controller gains	—
$\mathbf{K}_{\mathrm{geo}}{}^{\mathrm{e}}$	Element geometric matrix	—
K_g	Gain of the controller	—
$K_{v,D}$	Gain of velocity (or derivative) feedback controller	$\mathrm{Ns\,m^{-1}}$
k_{31}^2	The electro-mechanical coupling factor	—
k_B^*	Complex bending wave number (= $\left(m\omega^2/D_t^*\right)^{1/4}$)	$\mathrm{1\,m^{-1}}$
k_r	Ratio between derivative and proportional control gains	—
$k_{x,y}$	Wave numbers in the x and y directions	$\mathrm{1\,m^{-1}}$
$k_{r,i}$	Real and imaginary wave numbers	$\mathrm{1\,m^{-1}}$
$\bar{k}$	Dimensionless wave number (=$B_0 k$)	—
$[K]$	Stiffness matrix	$\mathrm{N\,m^{-1}}$
$[K_{e,s}]$	Elastic and structural stiffness matrices	$\mathrm{N\,m^{-1}}$
$[K_{I,R,v}]$	Imaginary, real, and VEM stiffness	$\mathrm{N\,m^{-1}}$
l_s	Sample thickness	m
L	Length, Laplace transform, Lagrangian	m
L	Electrical inductance	Henry
L_{ATF}	Proportionality constant of the ATF model	$\mathrm{m^2\,K^2\ (Ns)^{-1}}$
$\bar{L}$	Dimensionless electrical inductance (=L/R^2C^s)	—
M, m	Mass, electron mass	kg

(*Continued*)

Symbol	Meaning	Units
$M_{c,e}$	Control and external moments	Nm
$\mathbf{M}$	Magnetization	Amperes m^{-1}
$M_{x,y}$	Moments along the x and y directions	Nm
M_{ij}	Torsion moment in the i-j plane	Nm
$[M]$	Mass matrix	kg
$\{\mathbf{Mg}\}$	Global magnetization vector	Amperes m^{-1}
N	Number of mini-oscillators, Number of finite elements, Numerator	—
$N_{ix}, N_{i\theta}$	The longitudinal and tangential forces	N
N_{px}	Piezoelectric longitudinal control forces generated along the x-axis	N
$N_{x,y}$	Normal forces along the x and y directions	N
N_{ij}	Shear force in the i-j plane	N
$[N]$	Shape function of the finite element model	—
p_i	Internal normal forces per unit length	$\mathrm{N\,m}^{-1}$
P	Axial load	m
P_F	Active power (=*real* $[S_P]$)	$\mathrm{Nm\,s}^{-1}$
$P_{Fi,\ Fr}$	Instantaneous and reference active power flow	$\mathrm{Nm\,s}^{-1}$
$\{q\}$	Modal displacement vector	mrad
q_i	Externally applied body forces per unit length	$\mathrm{N\,m}^{-1}$
$\{q_{i,r}\}$	Imaginary and real modal displacement vectors	—
Q	Electrical charge	Coulomb
Q_F	Reactive power (=*imag* $[S_P]$)	$\mathrm{Nm\,s}^{-1}$
$Q_{x,y}$	The shear forces along the x,y directions	N
r	Scaled attenuation factor	—
R	Shell radius	m
R	Electrical resistance	ohm
R_a	Electrical resistance across filler particle	ohm
R_c	Contact electrical resistance between two filler particles	ohm
R_n	Eigenvector matrix of the n non-zero eigenvalues Λ	—
ΔR	Change in piezo-resistance of a conducting polymer	ohm
$[R_i]$	Rotation matrix	—
s	Laplace complex number	$\mathrm{rad\,s}^{-1}$
s	Separation distance between adjacent nano-particles	m
s_{11}^{D}	Compliance, in direction 1, at constant electric displacement, D	$\mathrm{m}^2\,\mathrm{N}^{-1}$
s_{11}^{E}	Compliance, in direction 1, at constant electric field, E	$\mathrm{m}^2\,\mathrm{N}^{-1}$

Symbol	Meaning	Units
s^{SH}	Compliance of the shunted network	m^2 N^{-1}
$[s^*]$	Overall compliance	m^2 N^{-1}
$[s_r^*]$	Compliance of the *rth* phase	m^2 N^{-1}
$[S^*]$	Eshleby strain tensor	—
$\mathbf{S}_{an}^e$	Magnetic stiffness matrix of the element	N m^{-1}
S_P	Complex vibrational power	Nm s^{-1}
t	Time	s
T	Temperature	°C
T	Kinetic energy	Nm
$T(t)$	A temporal function in, t	—
T_c	Internal axial tension	N
T_i	Stress on piezoelectric element along the *ith* direction	N m^{-2}
T_g	Glass transition temperature	°C
$[T]$	Transformation matrix	—
$[T_k]$	Transfer matrix for *kth* cell	—
$[T_r^*]$	Dilute concentration matrix	—
u,v,w	Deflections in the x, y, and z directions	m
$\hat{u}(x,\omega)$	Fourier transform of $u(x,t)$	ms
U	Potential energy	Nm
v, v_f	Volume fraction	—
$V_{c,s}$	Control and sensor voltages	V
$V_{x,y}$	Shear forces in the x and y directions	N
W	Energy dissipated of the viscoelastic material	Nm
$W(x)$	A spatial function in x	—
$W_{D,e}$	Dissipated and elastic energy	Nm
W_n	Nominal energy	Nm
W_{piezo}	Work done by the piezo-layer	Nm
$[W_r^*]$	Dilute concentration matrix	—
$\Delta W_{a,\ P}$	Dissipated energy due to active and passive damping	Nm
$\Delta W_{unconstrained}$	Dissipated energy due to unconstrained damping	Nm
x,y,z	Position	m
x_e	The “shear length” of a constrained damping treatment	m
X	Electrical reactance	ohm (Ω)
$\{X\}$	State vector	—
Y		—

(*Continued*)

Symbol	Meaning	Units
	The geometrical factor of a constrained damping treatment	
Y^D	Electrical admittance at constant electrical displacement, D	mho
Y^{EL}	Electrical admittance	mho
Y_F	Mobility	m (sN) $^{-1}$
Y^{SH}	Electrical shunted admittance	mho
z_i	*ith* internal degree of freedom of the VEM	—
Z^{EL}	Electrical impedance	ohm (Ω)
$\bar{Z}^{EL}$	Dimensionless electrical impedance (= Y^D/Y^{EL})	—
$(Z^{ME})^D$	Mechanical impedance at constant electrical displacement	Ns m^{-1}
Z^{ME}	Mechanical impedance	Ns m^{-1}
$(Z^{ME})^{SH}$	Mechanical impedance with electrical shunting	Ns m^{-1}
$\bar{Z}^{ME}$	Dimensionless mechanical impedance [$=(Z^{ME})^{SH}/(Z^{ME})^D$]	—

Greek Symbols

Symbol	Meaning	Units
α	Order of the fractional derivative	—
α	Attenuation factor	dB m^{-1}
α_n	Gain of GHM *nth* mini-oscillator	—
α_T	Temperature shift factor	—
β_i	The *ith* relative modulus of the GMM	—
β	weighting parameter of the Weighted Stiffness Matrix method (WSM)	—
γ	Shear strain, Localization factor, Lamé parameter	—
$\gamma_{a,\ p}$	Shear strain with active and passive treatments	—
γ_{ATF}	Effective modulus of the ATF model	N m^{-2} K^{-2}
$\Gamma(n)$	Gama function	—
$\langle\Gamma\rangle$	Average orientation	rad
δ	Phase shift due to damping (η = *tan* δ),	rad
δ_{ATF}	Coupling term between the mechanical displacement and the augmented temperature fields	N m^{-2} K^{-1}
Δ	The cubic dilation	—
Δ_{ATF}	Relaxation resistance of the ATF model	—

Symbol	Meaning	Units
$\{\Delta\}$	Deflection vector	mrad
ε	strain	—
$\bar{\varepsilon}$	Strain function of the fractional derivative method	—
ε^A	Applied strain	—
ε^C	Constrained strain	—
ε^T	Uniform transformation strain	—
$\boldsymbol{\varepsilon}_{33}^T$	Permittivity (or dielectric constant) in direction 3	Farad m^{-1}
$\hat{\varepsilon}(\omega)$	Fourier transform of the strain $\varepsilon(t)$	s
$[\bar{\varepsilon}_r]$	The average strain field in phase r	—
$[\varepsilon^0]$	Uniform elastic strain	—
ζ	Damping ratio	—
ζ_n	Damping ratio of GHM *nth* mini-oscillator,	—
	Damping ratio of the *nth* mode of vibration	—
η	Loss factor	—
η_n	Loss factor of the *nth* mode	—
η_v	Loss factor of the *VEM*	—
θ	Euler angle	rad
κ	Curvature	1/m
λ	Time constant ($\lambda = c_d/E_s$)	s
λ_B	Bending wavelength	m
Λ	Non-zero eigenvalues	rad s^{-1}
μ	Coefficient of friction, Propagation parameter and Lamé parameter (=G)	— N m^{-2}
μ_0	The permeability of space ($=4\pi \times 10^{-7}$)	T m A^{-1}
μ_r	The relative permeability of a magnetic material	Henry m^{-1}
ρ	Density	kg m^{-3}
ρ	Resistivity	ohm.m (Ω·m)
ρ_i	Relaxation time constant	s
ρ_{ATF_i}	Relaxation time constant of the ATF model	s
σ	Stress	N m^{-2}
$[\bar{\sigma}_r]$	The average stress field in phase, r	N m^{-2}
$[\sigma^0]$	Uniform elastic stress	N m^{-2}
τ	Time constant	s
τ_d	The dissipative shear stress in the VEM	N m^{-2}
τ_j	Retardation time	s
τ_{ij}	Shear stress in the *i-j* plane	N m^{-2}

(*Continued*)

Symbol	Meaning	Units
υ	Poisson's ratio	—
ϕ	Transformer turning ratio of piezo-element that transforms voltage into force $\left(=, -d_{31}A, /\left(s_{11}^{E}L\right)\right)$	$\mathrm{N\,V^{-1}}$
ϕ	Euler angle	rad
ϕ	Height of potential barrier between adjacent particles	eV
ϕ_n^*	The complex *nth* mode shape	—
$\phi_{n_{i,r}}$	imaginary and real components of the *nth* mode shape	—
Φ	Magnetic flux	Webers
$[\Phi]$	Mode shape matrix	—
Ψ	Shear strain of the stand-off layer	rad
$\Psi(t)$	Wavelet function	—
ω	Frequency	$\mathrm{rad\,s^{-1}}$
ω_n	Natural frequency	$\mathrm{rad\,s^{-1}}$
	Frequency of GHM *nth* mini-oscillator	$\mathrm{rad\,s^{-1}}$
ω_r	Reduced frequency ($=\alpha_T\omega$)	$\mathrm{rad\,s^{-1}}$
ω^*	Dimensionless length of damping treatment ($=L/B_0$)	—
Ω	Dimensionless frequency for VEM ($=\sqrt{(mh_1/G)}\,\omega$),	—
	Dimensionless frequency for resistive shunting ($=RC^S\omega$)	—

Subscripts

Symbol	Meaning
0	Initial value
d	Dissipative
e	Electrical
f	Friction
H	Hysteretic
i	Incident wave
o	Overall
p	Parallel, piezoelectric
r	Reflected waves
s	Elastic solid, series
sf	Strain free

Symbol	Meaning
stf	Stress free
S	Structural
t	Transmitted
v	Viscous

Superscripts

Symbol	Meaning
$*$	Complex conjugate
D	Constant electrical displacement
E	Constant electrical field
s	Constant strain
T	Transpose

Operators

Symbol	Meaning
$\lvert . \rvert$	Absolute value
$\lVert . \rVert$	Norm
$[.]^{-1}$	Inverse of the matrix [.] between the brackets
$[.]^T$	Transpose of the matrix [.] between the brackets
$\frac{d}{dx}(.)$	Differential operator with respect to x
$\frac{\partial}{\partial x}(.) = (.)_{,x}$	Partial differential operator with respect to x
$\dot{(.)} = \frac{d}{dt}(.)$	First derivative with respect to time
$\ddot{(.)} = \frac{d^2}{dt^2}(.)$	Second derivative with respect to time
$\delta(.)$	Variation of the quantity (.) between parentheses
$Re\ (.)$	Real part
$Im\ (.)$	Imaginary part

Abbreviations

ACLD	Active constrained layer damping
APDC	Active piezoelectric damping composites
ATF	Augmented temperature field
BVP	Boundary value problem
CLD	Constrained layer damping
DMTA	Dynamic mechanical thermal analysis
DOF	Degrees of freedom
DPM	Distributed-parameter model
EAP	Electroactive polymers
EDT	Engineered damping treatments
EMDC	Electromagnetic damping composites
FD	Fractional derivatives
FEM	Finite element method
FFT	Fast Fourier transform
FGM	Functionally graded material
GHM	Golla–Hughes–MacTavish model
G-L	Grunwald–Letnikov approach
GMC	Generalized method of cells
HTM	Halpin–Tsai method
IDOF	Internal degree of freedom of the VEM
IRS	Improved reduction system method
KE	Kinetic energy
LFA	Low frequency approximation method
LMS	Least mean square
MCLD	Magnetic constrained layer damping
MDR	Modal damping ratios
MMA	Method of moving asymptote
MR	Magnetorheological fluid
MSE	Modal strain energy
MTM	Mori–Tanaka method
MWCNT	Multi-walled carbon nanotubes
NSC	Negative stiffness composite

OC	Open circuit
P.E.	Potential energy
PCLD	Passive constrained layer damping
PVDF	Polyvinylidene fluoride
PZT	Lead zirconate titanate
R–L	The Reimann–Liouville approach
RVE	Representative volume element
SAFE	Semi-analytical finite element method
SC	Short circuit
SCM	Self-consistent method
SHPB	Split Hopkinson pressure bar
SOL	Stand-off layer
TTS	Time–temperature superposition
VAMUCH	Variational asymptotic method for unit cell homogenization
VEM	Viscoelastic material
WLF	Williams–Landel–Ferry formula
WSM	Weighted stiffness matrix method
WSTM	Weighted storage modulus method

Part I

Fundamentals of Viscoelastic Damping

1

Vibration Damping

1.1 Overview

Vibration control is recognized as an essential means for attenuating excessive amplitudes of oscillations, suppressing undesirable resonances, and avoiding premature fatigue failure of critical structures and structural components. The use of one form of vibration control or another in most of the newly designed structures is becoming very common in order to meet the pressing needs for large and light-weight structures. With such vibration control systems, the strict constraints imposed on present structures can be met to ensure their effective operation as quiet and stable platforms for manufacturing, communication, observation, and transportation.

1.2 Passive, Active, and Hybrid Vibration Control

Various passive, active, and hybrid vibration control approaches have been considered over the years employing a variety of structural designs, damping materials, active control laws, actuators, and sensors. Distinct among these approaches are the passive, active, and hybrid vibration damping methods.

It is important to note here that passive damping can be very effective in damping out high frequency excitations, whereas active damping can be utilized to control low frequency vibrations as shown in Figure 1.1. For effective control over broad frequency band, hybrid damping methods are essential.

1.2.1 Passive Damping

Passive damping treatments have been successfully used, for many years, to damp out the vibration of a wide variety of structures ranging from simple beams to complex space structures. Examples of such passive damping treatments include:

1.2.1.1 Free and Constrained Damping Layers

Both types of damping treatments rely in their operation on the use of a viscoelastic material (VEM) to extract energy from the vibrating structure as shown in Figure 1.2. In the free (or unconstrained) damping treatment, the vibrational energy is dissipated

Active and Passive Vibration Damping, First Edition. Amr M. Baz.
© 2019 John Wiley & Sons Ltd. Published 2019 by John Wiley & Sons Ltd.

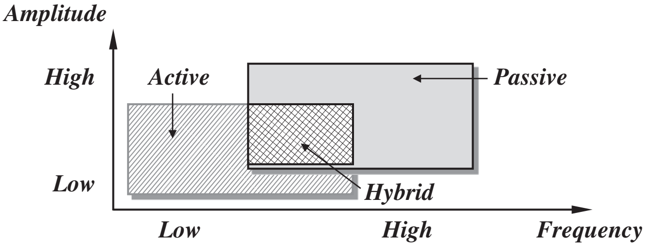

Figure 1.1 Operating range of various damping methods.

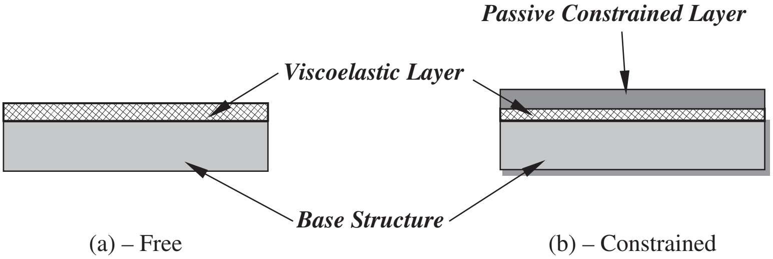
Passive Constrained Layer
Viscoelastic Layer
Base Structure
(a) – Free
(b) – Constrained

Figure 1.2 Viscoelastic damping treatments. (a) Free and (b) constrained.

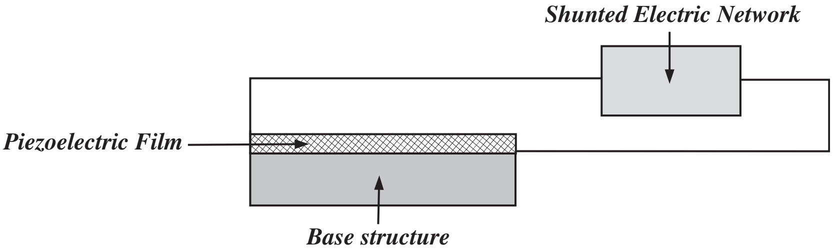
Shunted Electric Network
Piezoelectric Film
Base structure

Figure 1.3 Shunted piezoelectric treatments.

by virtue of the extensional deformation of the VEM, whereas in the constrained damping treatment more energy is dissipated through shearing the VEM (Nashif et al. 1985).

1.2.1.2 Shunted Piezoelectric Treatments

These treatments utilize piezoelectric films, bonded to the vibrating structure, to convert the vibrational energy into electrical energy. The generated energy is then dissipated in a shunted electric network, as shown in Figure 1.3, which are tuned in order to maximize the energy dissipation characteristics of the treatments (Lesieutre 1998). The electric networks are usually resistive, inductive, and/or capacitive. Other configurations of the shunted piezoelectric treatments include the viscoelastic polymer composites loaded with shunted piezoelectric inclusions introduced by Aldraihem et al. (2007).

1.2.1.3 Damping Layers with Shunted Piezoelectric Treatments

In these treatments, as shown in Figure 1.4, a piezoelectric film is used to passively constrain the deformation of a viscoelastic layer, which is bonded to a vibrating structure. The film is used also as a part of a shunting circuit that is tuned to improve the damping characteristics of the treatment over a wide operating range (Ghoneim 1995).

1.2.1.4 Magnetic Constrained Layer Damping (MCLD)

These treatments rely in their operation on arrays of specially arranged permanent magnetic strips that are bonded to viscoelastic damping layers. The interaction between the magnetic strips can improve the damping characteristics of the treatments by virtue of enhancing either the compression or the shear of the viscoelastic damping layers as shown in Figure 1.5.

In the compression MCLD configuration of Figure 1.5a, the magnetic strips (1 and 2) are magnetized across their thickness. Hence, the interaction between the strips generates magnetic forces that are perpendicular to the beam longitudinal axis. These forces subject the viscoelastic layer to across the thickness loading, which makes the treatment act like a Den–Hartog dynamic damper. In the shear MCLD configuration of Figure 1.5b, the magnetic strips (3 and 4) are magnetized along their length. Accordingly, the developed magnetic forces, which are parallel to the beam longitudinal axis, tend to shear the viscoelastic layer. In this configuration, the MCLD acts as conventional constrained layer

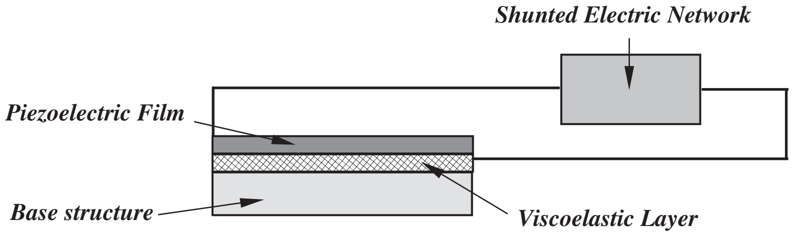

Figure 1.4 Damping layers with shunted piezoelectric treatments.

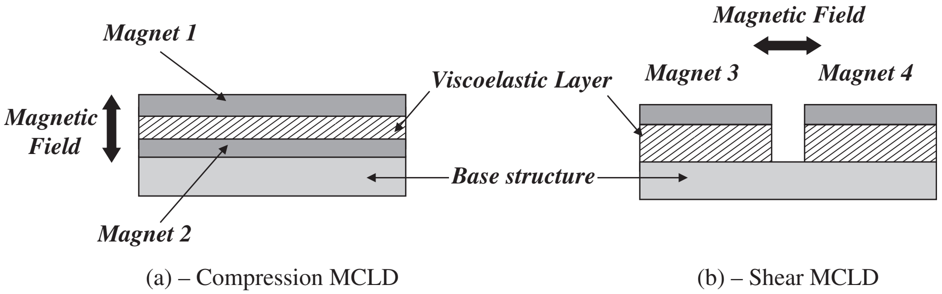

(a) – Compression MCLD (b) – Shear MCLD

Figure 1.5 Configurations of the MCLD treatment. (a) Compression MCLD and (b) shear MCLD.

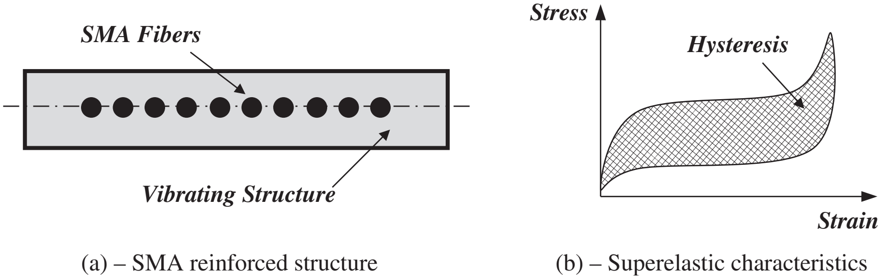

(a) – SMA reinforced structure (b) – Superelastic characteristics

Figure 1.6 Damping with shape memory fibers. (a) SMA reinforced structure and (b) superelastic characteristics.

damping treatment whose shear deformation is enhanced by virtue of the interaction between the neighboring magnetic strips (Baz 1997; Oh et al. 1999).

1.2.1.5 Damping with Shape Memory Fibers

This damping mechanism relies on embedding superelastic shape memory fibers in the composite fabric of the vibrating structures as shown in Figure 1.6a. The inherent hysteretic characteristics of the Shape Memory Alloy (SMA), in its superelastic form, are utilized to dissipate the vibration energy. The amount of energy dissipated is equal to the area enclosed inside the stress–strain characteristics (Figure 1.6b). This passive mechanism has been successfully used in damping out the vibration of a wide variety of structures including large structures subject to seismic excitation (Greaser and Cozzarelli 1993).

1.2.2 Active Damping

Although the passive damping methods described here are simple and reliable, their effectiveness is limited to a narrow operating range because of the significant variation of the damping material properties with temperature and frequency. It is, therefore, difficult to achieve optimum performance with passive methods alone particularly over wide operating conditions.

Hence, various active damping methods have been considered. All of these methods utilize control actuators and sensors of one form or another. The most common types are made of piezoelectric films bonded to the vibrating structure as shown in Figure 1.7.

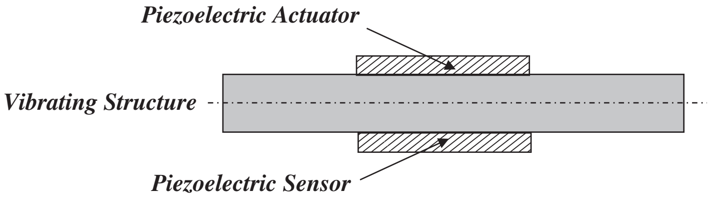

Figure 1.7 Active damping.

This active control approach has been successfully used in damping out the vibration of a wide variety of structures ranging from simple beams to more complex space structures (Preumont 1997; Forward 1979).

1.2.3 Hybrid Damping

Because of the limited control authority of the currently available active control actuators, and because of the limited effective operating range of passive control methods, treatments that are a hybrid combination of active damping and passive damping treatments have been considered. Such hybrid treatments aim to use various active control mechanisms to augment the passive damping in a way that compensates for its performance degradation with temperature and/or frequency. Also, these treatments combine the simplicity of passive damping with the effectiveness of active damping in order to ensure optimal blend of the favorable attributes of both damping mechanisms.

Among the most commonly used hybrid treatments are:

1.2.3.1 Active Constrained Layer Damping (ACLD)

This class of treatments is a blend between a passive constrained layer damping and active piezoelectric damping as shown in Figure 1.8. Here, the piezo-film is actively strained in such a manner to enhance the shear deformation of the viscoelastic damping layer in response to the vibration of the base structure (Baz 1996, 2000; Crassidis et al. 2000).

1.2.3.2 Active Piezoelectric Damping Composites (APDC)

In this class of treatments, an array of piezo-ceramic rods embedded across the thickness of a viscoelastic polymeric matrix are electrically activated to control the damping characteristics of the matrix that is directly bonded to the vibrating structure as shown in Figure 1.9. The figure displays two arrangements of the APDC. In the first arrangement, the piezo-rods are embedded perpendicular to the electrodes to control the compressional damping (Reader and Sauter 1993) and in the second arrangement, the rods

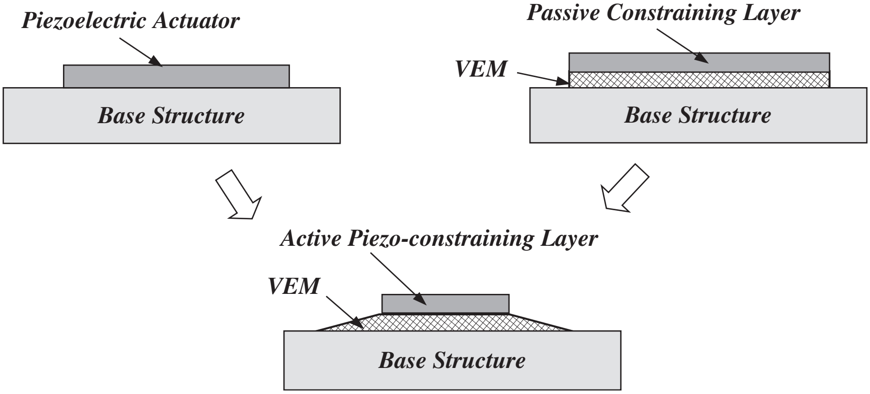

Figure 1.8 Active constrained layer damping treatment.

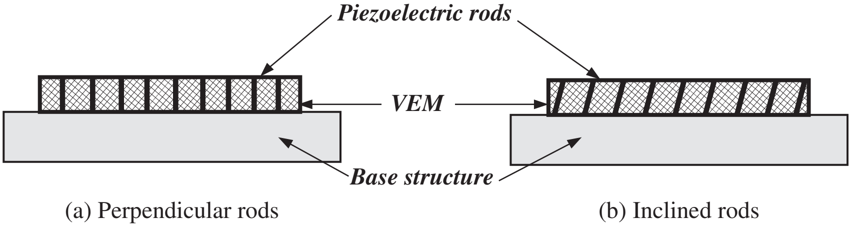

Figure 1.9 Active piezoelectric damping composites. (a) Perpendicular rods and (b) inclined rods.

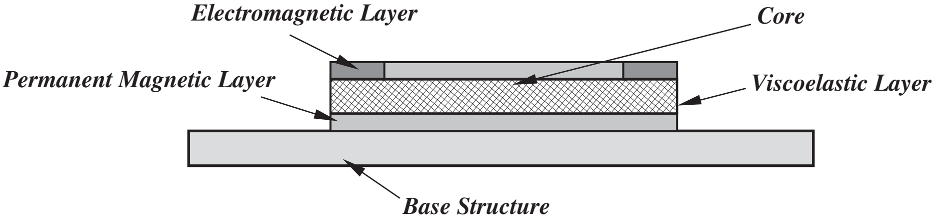

Figure 1.10 Electromagnetic damping composite (EMDC).

are obliquely embedded to control both the compressional and shear damping of the matrix (Baz and Tampia 2004; Arafa and Baz 2000).

1.2.3.3 Electromagnetic Damping Composites (EMDC)

In this class of composites, a layer of viscoelastic damping treatment is sandwiched between a permanent and electromagnetic layer as shown in Figure 1.10. The entire assembly is bonded to the vibrating surface to act as a smart damping treatment. The interaction between the magnetic layers, in response to the structural vibration, subjects the viscoelastic layer to compressional forces of proper magnitude and phase shift. These forces counterbalance the transverse vibration of the base structure and enhance the damping characteristics of the VEM. Accordingly, the electromagnetic damping composite (EMDC) acts in effect as a tunable Den–Hartog damper with the base structure serving as the primary system, the electromagnetic layer acting as the secondary mass, the magnetic forces generating the adjustable stiffness characteristics, and the viscoelastic layer providing the necessary damping effect (Baz 1997; Omer and Baz 2000; Ruzzene et al. 2000; Baz and Poh 2000; Oh et al. 2000).

1.2.3.4 Active Shunted Piezoelectric Networks

In this class of treatments, shown schematically in Figure 1.11, the passive shunted electric network is actively switched on and off in response to the response of the structure/network system in order to maximize the instantaneous energy dissipation characteristics and minimize the frequency-dependent performance degradation (Lesieutre 1998; Tawfik and Baz 2004; Park and Baz 2005; Thorp et al. 2005).

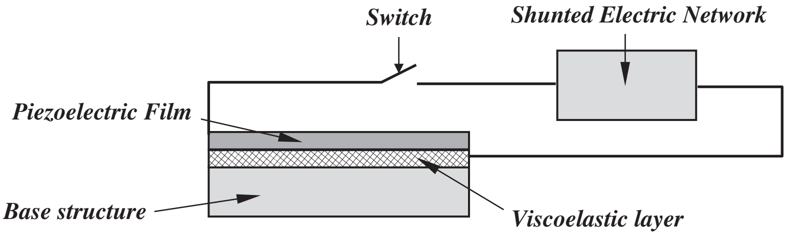

Figure 1.11 Damping layers with shunted piezoelectric treatments.

1.3 Summary

This chapter has presented a brief description of the main vibration control methods that have been successfully applied to damping out the vibration of a wide variety of structures. Analysis and performance characteristics of these vibration damping control methods will be presented in the remaining chapters.

References

Aldraihem, O., Baz, A., and Al-Saud, T.S. (2007). Hybrid composites with shunted piezoelectric particles for vibration damping. *Journal of Mechanics of Advanced Materials and Structures* 14: 413–426.

Arafa, M. and Baz, A. (2000). Dynamics of active piezoelectric damping composites. *Journal of Composites Engineering: Part B* 31: 255–264.

Baz A. Active Constrained Layer Damping, US Patent 5,485,053, filed October 15 1993 and issued January 16 1996.

Baz A. “Magnetic constrained layer damping”, Proceedings of 11th Conference on Dynamics & Control of Large Structures, Blacksburg, VA (May 1997), pp. 333–344.

Baz, A. (2000). Spectral finite element modeling of wave propagation in rods using active constrained layer damping. *Journal of Smart Materials and Structures* 9: 372–377.

Baz, A. and Poh, S. (2000). Performance characteristics of magnetic constrained layer damping. *Journal of Shock & Vibration* 7 (2): 18–90.

Baz, A. and Tampia, A. (2004). Active piezoelectric damping composites. *Journal of Sensors and Actuators: A. Physical* 112 (2–3): 340–350.

Crassidis, J., Baz, A., and Wereley, N. (2000). H_∞ control of active constrained layer damping. *Journal of Vibration & Control* 6 (1): 113–136.

Forward, R.L. (1979). Electronic damping of vibrations in optical structures. *Applied Optics* 18 (5): 1.

Ghoneim H. “Bending and twisting vibration control of a cantilever plate via electromechanical surface damping”. Proceedings of the Smart Structures and Materials Conference (ed. C. Johnson), Vol. SPIE-2445, pp. 28–39, 1995.

Greaser E. and Cozzarelli F., "Full cyclic hysteresis of a Ni-Ti shape memory alloy", Proceedings of DAMPING '93 Conference, San Francisco, CA, Wright Laboratory Document no. WL-TR-93-3105, Vol. 2, pp. ECB-1–28, 1993.

Lesieutre, G.A. (1998). Vibration damping and control using shunted piezoelectric materials. *The Shock and Vibration Digest* 30 (3): 187–195.

Nashif, A., Jones, D., and Henderson, J. (1985). *Vibration Damping*. New York: Wiley.

Oh, J., Ruzzene, M., and Baz, A. (1999). Control of the dynamic characteristics of passive magnetic composites. *Journal of Composites Engineering, Part B* 30: 739–751.

Oh, J., Poh, S., Ruzzene, M., and Baz, A. (2000). Vibration control of beams using electromagnetic compressional damping treatment. *ASME Journal of Vibration & Acoustics* 122 (3): 235–243.

Omer, A. and Baz, A. (2000). Vibration control of plates using electromagnetic compressional damping treatment. *Journal of Intelligent Material Systems & Structures* 11 (10): 791–797.

Park, C.H. and Baz, A. (2005). Vibration control of beams with negative capacitive shunting of interdigital electrode piezoceramics. *Journal of Vibration and Control* 11 (3): 331–346.

Preumont, A. (1997). *Vibration Control of Active Structures*. Dordrecht, The Netherlands: Kluwer Academic Publishers.

Reader W. and Sauter D., "Piezoelectric composites for use in adaptive damping concepts", Proceedings of DAMPING '93, San Francisco, CA (February 24–26, 1993), pp. GBB 1–18.

Ruzzene, M., Oh, J., and Baz, A. (2000). Finite element modeling of magnetic constrained layer damping. *Journal of Sound & Vibration* 236 (4): 657–682.

Tawfik, M. and Baz, A. (2004). Experimental and spectral finite element study of plates with shunted piezoelectric patches. *International Journal of Acoustics and Vibration* 9 (2): 87–97.

Thorp, O., Ruzzene, M., and Baz, A. (2005). Attenuation of wave propagation in fluid-loaded shells with periodic shunted piezoelectric rings. *Journal of Smart Materials & Structures* 14 (4): 594–604.

2

Viscoelastic Damping

2.1 Introduction

Viscoelastic damping treatments have been extensively used in various structural applications to control undesirable vibrations and associated noise radiation in a simple and reliable manner (Nashif et al. 1985; Sun and Lu 1995). In this chapter, particular emphasis is placed on studying the dynamic characteristics of such damping treatments and outlining the different mathematical models used to describe the behavior of these treatments over a wide range of operating frequencies and temperatures. Particular focus is given to ascertain the merits and drawbacks of the classical models by Maxwell, Kelvin–Voigt, and Zener (Zener 1948; Flugge 1967; Christensen 1982; Haddad 1995; Lakes 1999, 2009) both in the time and frequency domains.

2.2 Classical Models of Viscoelastic Materials

These models include the of Maxwell, Kelvin–Voigt, and Poynting–Thomson models (Haddad 1995; Lakes 1999, 2009). In these models, the dynamics of **V**isco**E**lastic **M**aterials (VEMs) are described in terms of series and/or parallel combinations of viscous dampers and elastic springs as shown in Figure 2.1. The dampers are included to capture the viscous behavior of the VEM, whereas the springs are used to simulate the elastic behavior of the VEM.

2.2.1 Characteristics in the Time Domain

The dynamic characteristics of Maxwell and Kelvin–Voigt models in the time domain are summarized in Table 2.1.

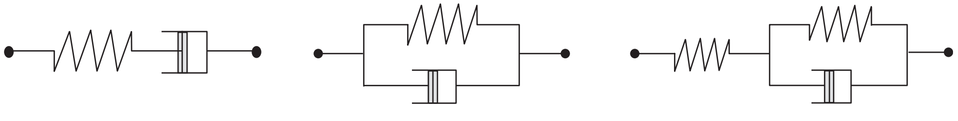
(a) – Maxwell Model
(b) – Kelvin-Voigt Model
(c) – Poynting-Thomson Model

Figure 2.1 Classical models of VEMs. (a) Maxwell model, (b) Kelvin–Voigt model, and (c) Poynting–Thomson model.

Active and Passive Vibration Damping, First Edition. Amr M. Baz.
© 2019 John Wiley & Sons Ltd. Published 2019 by John Wiley & Sons Ltd.

Table 2.1 The dynamic equations of Maxwell and Kelvin–Voigt models.

Model	Maxwell model	Kelvin–Voigt model
Stresses and strains of components	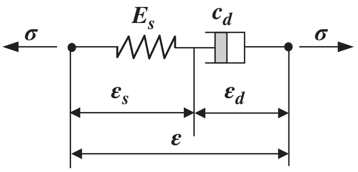 E_s c_d σ σ ε_s ε_d ε	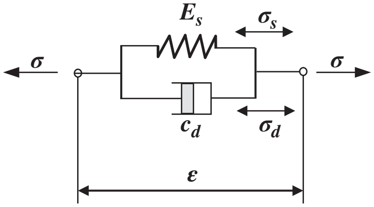 E_s σ_s σ σ c_d σ_d ε
Equilibrium and kinematic equations	- Stress σ is same for spring and damper - Strain ε is sum of strains of spring and damper: $\sigma = \sigma_s = \sigma_d$ (2.1) and $\varepsilon = \varepsilon_s + \varepsilon_d$ (2.3)	- Strain ε is same for spring and damper - Stress σ is sum of stresses of spring and damper: $\sigma = \sigma_s + \sigma_d$ (2.2) and $\varepsilon = \varepsilon_s = \varepsilon_d$ (2.4)
Constitutive equations	**Spring**: $\sigma = E_s \varepsilon_s$ (2.5) **Damper**: $\sigma = c_d \dot{\varepsilon}_d$ (2.7)	**Spring**: $\sigma_s = E_s \varepsilon$ (2.6) **Damper**: $\sigma_d = c_d \dot{\varepsilon}$ (2.8)
Model equation	Substituting Eqs. (2.5) and (2.7) into Eq. (2.3) gives: $\lambda\dot{\sigma} + \sigma = c_d \dot{\varepsilon}$ (2.9) where $\lambda = c_d/E_s$	Substituting Eqs. (2.6) and (2.8) into Eq. (2.2) gives: $\sigma = E_s \varepsilon + c_d \dot{\varepsilon}$ (2.10)

(E_s = Young's modulus of elastic element, c_d = damping coefficient of dissipative element)

One can note that the stress–strain equations of the Maxwell and Kelvin–Voigt models can generally be written as follows:

$$P\sigma = Q\varepsilon \tag{2.11}$$

where P and Q are differential operators given by:

$$P = \sum_{i=0}^{p} \alpha_i \frac{d^i}{dt^i} \text{ and } Q = \sum_{j=0}^{q} \beta_j \frac{d^j}{dt^j} \tag{2.12}$$

Hence, for Maxwell model, $p = 1$, $q = 1$, $\alpha_0 = 1$, $\alpha_1 = \lambda$, $\beta_0 = 0$ and $\beta_1 = c_d$ while for the Kelvin–Voigt model, $p = 0$, $q = 1$, $\alpha_0 = 1$, $\beta_0 = E_s$ and $\beta_1 = c_d$.

The ability of both the Maxwell and the Kelvin–Voigt models to predict the characteristics of realistic VEM will be determined by considering the behavior under creep and relaxation loading conditions.

2.2.2 Basics for Time Domain Analysis

The initial and final value theorems of the Laplace transform are essential to the complete understanding of the behavior of viscoelastic models in the time domain. Appendix 2.A summarizes the two theorems and presents the necessary proofs.

Application of these two theorems to Maxwell and Kelvin–Voigt models is summarized in Tables 2.2 and 2.3 when these models are subjected to creep and relaxation

Table 2.2 Initial and final values of stresses and strains of Maxwell and Kelvin–Voigt models when subjected to creep loading.

Model	Maxwell model	Kelvin–Voigt model
Model	$\lambda\dot{\sigma} + \sigma = c_d\dot{\varepsilon}$	$\sigma = E_s\varepsilon + c_d\dot{\varepsilon}$
Loading conditions	The stress is constant $\sigma = \sigma_0$ and the initial and final values of the strain ε are predicted. 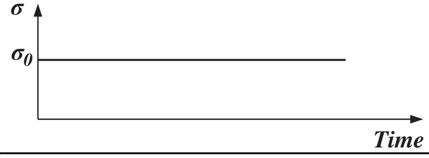 	
The strain in the Laplace s domain	$\varepsilon = \frac{\lambda s + 1}{c_d s}\sigma = \frac{\lambda s + 1}{c_d s^2}\sigma_0$	$\varepsilon = \frac{1}{E_s(\lambda s + 1)}\sigma = \frac{1}{E_s s(\lambda s + 1)}\sigma_0$
Initial value	$\begin{aligned}\varepsilon_0 &= \lim_{s\to\infty} s\varepsilon \\ &= \lim_{s\to\infty} \frac{\lambda + 1/s}{c_d}\sigma_0 = \frac{\sigma_0}{E_s}\end{aligned}$	$\begin{aligned}\varepsilon_0 &= \lim_{s\to\infty} s\varepsilon \\ &= \lim_{s\to\infty} \frac{1}{E_s(\lambda s + 1)}\sigma_0 = 0\end{aligned}$
Final value	$\begin{aligned}\varepsilon_\infty &= \lim_{s\to 0} s\varepsilon \\ &= \lim_{s\to 0} \frac{\lambda s + 1}{c_d s}\sigma_0 = \infty\end{aligned}$	$\begin{aligned}\varepsilon_\infty &= \lim_{s\to 0} s\varepsilon \\ &= \lim_{s\to 0} \frac{1}{E_s(\lambda s + 1)}\sigma_0 = \frac{\sigma_0}{E_s}\end{aligned}$

Table 2.3 Initial and final values of stresses and strains of Maxwell and Kelvin–Voigt models when subjected to relaxation loading.

Model	Maxwell model	Kelvin–Voigt model
Model	$\lambda\dot{\sigma} + \sigma = c_d\dot{\varepsilon}$	$\sigma = E_s\varepsilon + c_d\dot{\varepsilon}$
Loading conditions	The strain is constant $\varepsilon = \varepsilon_0$ and the initial and final values of the stress σ are predicted. 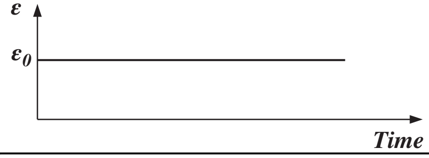 	
The stress in the Laplace s domain	$\sigma = \frac{c_d s}{\lambda s + 1}\varepsilon = \frac{c_d}{\lambda s + 1}\varepsilon_0$	$\sigma = E_s(\lambda s + 1)\varepsilon = \frac{E_s(\lambda s + 1)}{s}\varepsilon_0$
Initial value	$\begin{aligned}\sigma_0 &= \lim_{s\to\infty} s\sigma \\ &= \lim_{s\to\infty} \frac{c_d s}{\lambda s + 1}\varepsilon_0 = E_s\varepsilon_0\end{aligned}$	$\begin{aligned}\sigma_0 &= \lim_{s\to\infty} s\sigma \\ &= \lim_{s\to\infty} E_s\varepsilon_0 = E_s\varepsilon_0\end{aligned}$
Final value	$\begin{aligned}\sigma_\infty &= \lim_{s\to 0} s\sigma \\ &= \lim_{s\to 0} \frac{c_d s}{\lambda s + 1}\varepsilon_0 = 0\end{aligned}$	$\begin{aligned}\sigma_\infty &= \lim_{s\to 0} s\sigma \\ &= \lim_{s\to 0} E_s\varepsilon_0 = E_s\varepsilon_0\end{aligned}$

loading, respectively. These two theorems provide the means for determining the initial and final limits of the VEM response under different loading conditions. This feature enables the correct calculation of the time response, between these two limits, when the differential equations describing these models are solved as will be demonstrated later.

Table 2.2 indicates that the Maxwell model experiences an initial strain when the creep load is applied, which is typical in VEMs. However, this strain tends to become unbounded as time grows. This feature is not observed or supported experimentally. As for the Kelvin–Voigt model, the initial value theorem indicates zero initial strain, which is rather unrealistic and a bounded final strain of σ_0/E_s that is observed in a realistic VEM.

Table 2.3 indicates that the Maxwell model experiences an initial stress when the relaxation strain is applied and that stress is completely relieved as time progresses. Both of these characteristics are typical in VEM. As for the Kelvin–Voigt model, the initial and the final values remain constant $E_s\varepsilon_0$, which is rather unrealistic behavior of a VEM.

2.2.3 Detailed Time Response of Maxwell and Kelvin–Voigt Models

Tables 2.4 and 2.5 summarize the detailed behavior characteristics of Maxwell and Kelvin–Voigt models in the time domain between the initial and final values predicted in Tables 2.2 and 2.3.

Tables 2.4 and 2.5 indicate that the Maxwell model predicts unrealistic creep characteristics as the strain tends to be unbounded even for finite stress levels or the strain tends to remain constant when the stress is removed. The Kelvin–Voigt model also yields unrealistic relaxation characteristics with the stress remaining constant with time, indicating that the VEM does not exhibit any stress relaxation. Therefore, neither the Maxwell nor the Kelvin–Voigt model replicates the behavior of realistic VEM.

Note that these predictions, particularly at $t = 0$, are in agreement with the predictions of the initial and final value theorems listed in Tables 2.2 and 2.3.

In order to avoid the drawbacks and limitations of both the Maxwell and Kelvin–Voigt models, several other spring-damper arrangements have been considered. For example, a damper with series and parallel springs is considered to combine the attractive attributes and compensate for the deficiencies of both the Maxwell and Kelvin–Voigt models. The resulting model is the *Poynting–Thomson* model, shown in Figures 2.1c and 2.2a. Other common models are also displayed in Figure 2.2 such the "three-parameter model" and the "standard solid model" (Zener 1948).

Figure 2.3a,b show the most widely used spring-mass configurations of VEM models that are employed extensively, particularly, in commercial finite element packages. These two configurations are, namely, the generalized Maxwell model and the generalized Kelvin–Voigt model.

These two generalized *n* classical models are assembled in parallel or series to model the complex behavior of realistic VEMs. These models are augmented with additional springs E_0, either in parallel or series, to eliminate the drawbacks associated with the classical models as outlined in Tables 2.2–2.5.

Table 2.4 The creep characteristics of Maxwell and Kelvin–Voigt models.

Model	Maxwell model	Kelvin–Voigt model
Loading conditions	The stress is constant $\sigma = \sigma_0$ and the time history of the strain is predicted 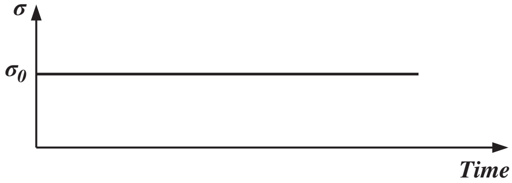 	
Response	• As the initial strain $\varepsilon = \varepsilon_0{}^a$ at time $t = 0$, • Hence: $\varepsilon = \frac{\sigma_0}{c_d}t + \frac{\sigma_0}{E_s} = \frac{\sigma_0}{E_s}(1 + t/\lambda)$ (2.13) 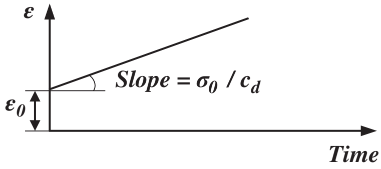 • Unbounded strain for bounded stress	• As the initial strain $\varepsilon = 0^a$ at time t = 0, • Hence: $\varepsilon = \frac{\sigma_0}{E_s}\left[1 - e^{-t/\lambda}\right]$ (2.14) 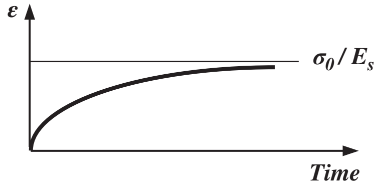 • Bounded strain for bounded stress
Unloading Conditions	The stress is reduced back to zero at time $t = t_1$ and the time history of the strain 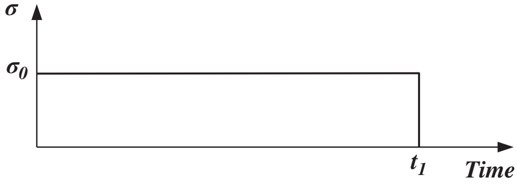 	
Response	• At $t = t_1$, $\varepsilon_1 = \frac{\sigma_0}{c_d}t_1 + \frac{\sigma_0}{E_s}$, • Hence, when $\sigma = 0$: $\dot{\varepsilon} = 0$ with solution $\varepsilon = \varepsilon_1$= constant (2.15) 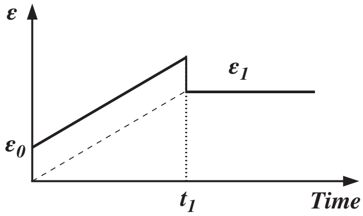 • No contraction after stress removal	• At $t = t_1$, $\varepsilon_1 = \frac{\sigma_0}{E_s}\left[1 - e^{-t_1/\lambda}\right]$, • Hence, when $\sigma = 0$: $E_s\varepsilon + c_d\dot{\varepsilon} = 0$ or $\lambda\dot{\varepsilon} + \varepsilon = 0$ with solution $\varepsilon = \varepsilon_1 e^{-(t-t_1)/\lambda}$ (2.16) 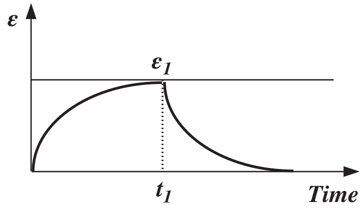 • Complete strain relief after stress removal

[a] Table 2.2 (using initial value theorem).

Table 2.5 Relaxation characteristics of Maxwell and Kelvin–Voigt models.

Model	Maxwell model	Kelvin–Voigt model
Loading conditions	The strain is constant $\varepsilon = \varepsilon_0$ and determines the time history of the stress 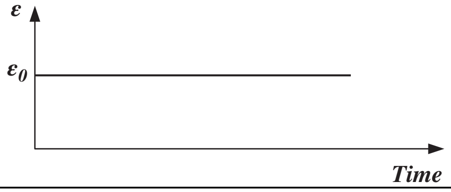 	
Response	As the initial stress $\sigma = \sigma_0{}^a$ at time $t = 0$: Hence: $\lambda\dot{\sigma} + \sigma = 0$ with solution $\sigma = E_s e^{-t/\lambda}\varepsilon_0$ (2.17) 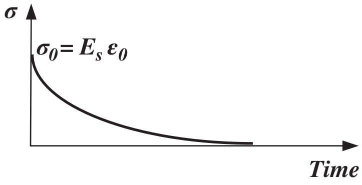 stress decays to zero without any residual stress	As the initial strain $\varepsilon = \varepsilon_0{}^a$ at time $t = 0$: Hence: $\sigma = E_s\varepsilon_0 = \text{constant}$ (2.18) 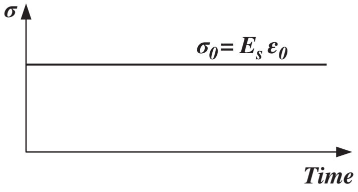 stress remains constant, that is, VEM exhibits no relaxation

[a] Table 2.3 (using initial value theorem).

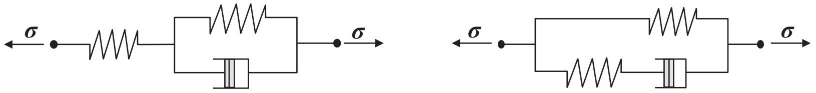

(a) – Poynting-Thomson Model (b) – Zener Model

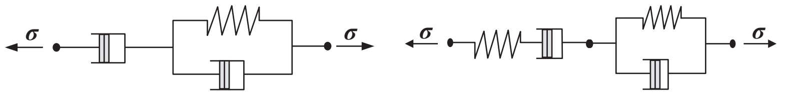

(c) – Jeffrey Model (d) – Burgers Model

Figure 2.2 Other common viscoelastic models. (a) Poynting–Thomson model, (b) Zener model, (c) Jeffrey model, and (d) Burgers model.

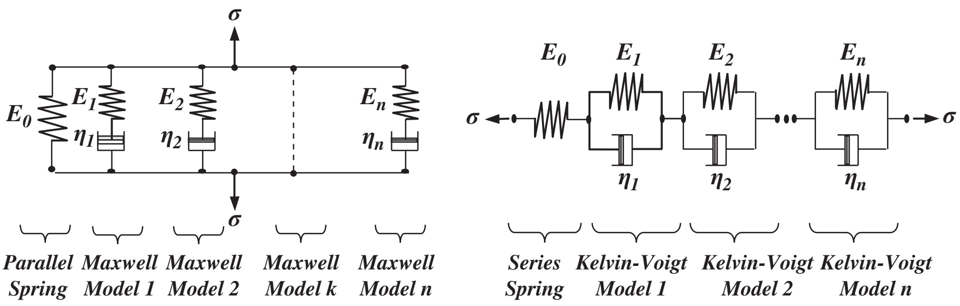
σ
E0
E1
η1
E2
η2
En
ηn
σ
Parallel Spring
Maxwell Model 1
Maxwell Model 2
Maxwell Model k
Maxwell Model n
E0
E1
E2
En
σ
σ
η1
η2
ηn
Series Spring
Kelvin-Voigt Model 1
Kelvin-Voigt Model 2
Kelvin-Voigt Model n

(a) (b)

Figure 2.3 Generalized Maxwell (a) and Kelvin–Voigt (b) models.

2.2.4 Detailed Time Response of the Poynting–Thomson Model

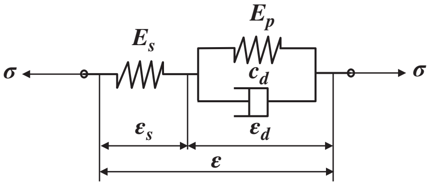

Figure 2.4 Poynting–Thomson viscoelastic model.

The stress σ across the series spring of the Poynting–Thomson model, shown in Figure 2.4, is given by:

$$\sigma = E_s \varepsilon_s \tag{2.19}$$

and the stress σ across the damper and the parallel spring is given by:

$$\sigma = E_p \varepsilon_d + c_d \dot{\varepsilon}_d \tag{2.20}$$

Using the Laplace transformation, yields

$$\varepsilon_s = \sigma / E_s \text{ and } \varepsilon_d = \sigma / \left(E_p + c_d s\right) \tag{2.21}$$

Hence, the total strain ε across the Poynting–Thomson model is

$$\varepsilon = \varepsilon_s + \varepsilon_d = \left[\frac{\left(E_s + E_p\right) + c_d s}{E_s\left(E_p + c_d s\right)}\right] \sigma \tag{2.22}$$

In the time domain, this equation becomes

$$\left(E_s + E_p\right)\sigma + c_d \dot{\sigma} = E_s E_p \varepsilon + E_s c_d \dot{\varepsilon} \tag{2.23}$$

From Eqs. (2.11), (2.12), and (2.23), $p = 1$, $q = 1$, $\alpha_0 = (E_s + E_p)$, $\alpha_1 = c_d$, $\beta_0 = E_s E_p$, and $\beta_1 = E_s c_d$.

a) *The creep characteristics of the Poynting–Thomson model* are obtained as follows:

i) Determine the initial and final values strain:

For stress $\sigma = \sigma_0$, then Eq. (2.22) reduces to:

$$\varepsilon = \left[\frac{\left(E_s + E_p\right) + c_d s}{E_s\left(E_p + c_d s\right)}\right] \frac{\sigma_0}{s}$$

Then,

$$\varepsilon_0 = \lim_{s \to \infty} s\varepsilon = \lim_{s \to \infty} \left[\frac{\left(E_s + E_p\right) + c_d s}{E_s\left(E_p + c_d s\right)}\right] \sigma_0 = \frac{\sigma_0}{E_s}$$

and

$$\varepsilon_\infty = \lim_{s \to 0} s\varepsilon = \lim_{s \to 0} \left[\frac{\left(E_s + E_p\right) + c_d s}{E_s\left(E_p + c_d s\right)}\right] \sigma_0 = \frac{\sigma_0}{E_\infty}$$

where $E_\infty = \dfrac{E_s E_p}{\left(E_s + E_p\right)}$.

ii) Determine the time history of the strain:

The time history of the strain is determined by solving Eq. (2.23) such that at $t = 0$, $\sigma = \sigma_0$, and the initial strain $\varepsilon_0 = \sigma_0/E_s$. Hence, Eq. (2.23) reduces to:

$$E_s c_d \dot{\varepsilon} + E_s E_p \varepsilon = \left(E_s + E_p\right)\sigma_0$$

This equation has a solution:

$$\varepsilon = \frac{\sigma_0}{E_\infty}\left[1 + \frac{E_\infty - E_s}{E_s} e^{-t/\lambda}\right] \tag{2.24}$$

where $\lambda = c_d/E_p$ and $E_\infty = E_s E_p/(E_s + E_p)$. Note that Eq. (2.24) has the initial and final values ε_0 and ε_∞ at $t = 0$ and $t = \infty$.

Figure 2.5 shows the strain–time characteristics as predicted by Eq. (2.24).

b) *The Relaxation characteristics of the Poynting–Thomson model* are obtained as follows:

i) Determining the initial and final values stress:

For strain $\varepsilon = \varepsilon_0$, then Eq. (2.22) reduces to:

$$\sigma = \left[\frac{E_s\left(E_p + c_d s\right)}{\left(E_s + E_p\right) + c_d s}\right]\frac{\varepsilon_0}{s}$$

Then,

$$\sigma_0 = \lim_{s\to\infty} s\sigma = \lim_{s\to\infty}\left[\frac{E_s\left(E_p + c_d s\right)}{\left(E_s + E_p\right) + c_d s}\right]\varepsilon_0 = E_s\varepsilon_0$$

and

$$\sigma_\infty = \lim_{s\to 0} s\varepsilon = \lim_{s\to 0}\left[\frac{E_s\left(E_p + c_d s\right)}{\left(E_s + E_p\right) + c_d s}\right]\varepsilon_0 = E_\infty\varepsilon_0$$

where $E_\infty = \dfrac{E_s E_p}{\left(E_s + E_p\right)}$.

ii) Determining the time history of the stress:

The time history of the stress can be determined by solving Eq. (2.23) such that at $t = 0$, $\varepsilon = \varepsilon_0$, and the initial stress $\sigma_0 = E_s\varepsilon_0$. Hence, Eq. (2.23) reduces to:

$$c_d\dot{\sigma} + \left(E_s + E_p\right)\sigma = E_s E_p \varepsilon_0$$

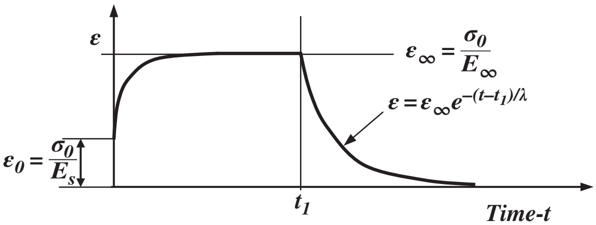

Figure 2.5 The creep characteristics of the Poynting–Thomson model.

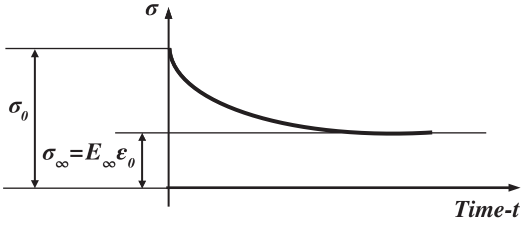

Figure 2.6 The relaxation characteristics of the Poynting–Thomson model.

This equation has the following solution:

$$\sigma = E_\infty \varepsilon_0 \left[\left(1 - e^{-t/\alpha} \right) \right] + E_s \varepsilon_0 \, e^{-t/\alpha} \tag{2.25}$$

where $\alpha = \dfrac{c_d}{\left(E_s + E_p\right)}$.

Figure 2.6 shows the stress–time characteristics as predicted by Eq. (2.25).

Table 2.6 summarizes the main characteristics of Maxwell, Kelvin–Voigt, and Poynting–Thomson models.

The characteristics summarized in Table 2.6 ascertain the ability of the Poynting–Thomson model to simulate a realistic behavior of VEMs. However, several

Table 2.6 Time domain characteristics of classical viscoelastic models.

Parameter	**Maxwell**	**Kelvin–Voigt**	**Poynting–Thomson**
Model	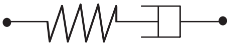	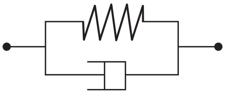	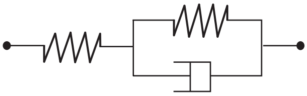
Dynamic equations	$\lambda \dot{\sigma} + \sigma = c_d \dot{\varepsilon}$	$\sigma = E_s \varepsilon + c_d \dot{\varepsilon}$	$\left(E_s + E_p\right)\sigma + c_d \dot{\sigma} = E_s E_p \varepsilon + E_s c_d \dot{\varepsilon}$
Creep characteristics	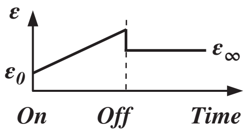	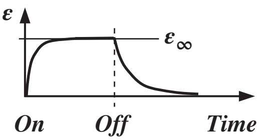	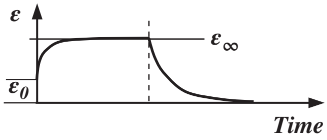
Comments	Unrealistic	Realistic	Realistic
Relaxation characteristics	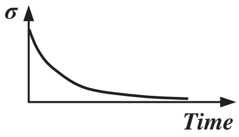	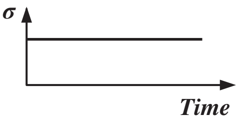	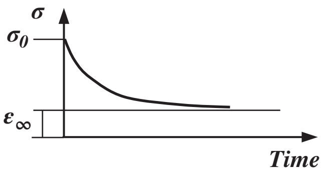
Comments	Realistic	Unrealistic	Realistic

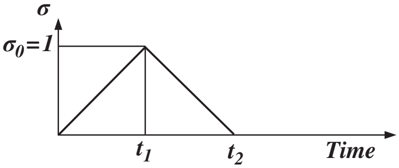

Figure 2.7 A ramp creep loading and loading cycle.

Table 2.7 Solutions of the constitutive equations.

Parameter	Maxwell	Kelvin–Voigt
Constitutive equation	$\dot{\varepsilon} = \dot{\sigma} + \sigma$	$\dot{\varepsilon} + \varepsilon = \sigma$
Equation during loading	$\dot{\varepsilon} = 1 + t$	$\dot{\varepsilon} + \varepsilon = t$
Initial condition (ε_0)	$\varepsilon_0 = 0$	$\varepsilon_0 = 0$
Response	$\varepsilon = \varepsilon_0 + t + {}^1/_2 t^2$	$\varepsilon = (\varepsilon_0 + 1)e^{-t} - 1 + t$
Equation during unloading	$\dot{\varepsilon} = 1 - t$	$\dot{\varepsilon} + \varepsilon = 2 - t$
Initial condition (ε_1)	$\varepsilon_1 = 1.5$	$\varepsilon_1 = e^{-1}$
Response	$\varepsilon = 1 + t - {}^1/_2 t^2$	$\varepsilon = 3 - t + e^{-t} - 2e^{1-t}$

combinations of Poynting–Thomson models are necessary to replicate the behavior of realistic VEMs.

Example 2.1 Plot the stress–strain characteristics for the Maxwell and Kelvin–Voigt models when the VEM is subjected to the loading and unloading cycle shown in Figure 2.7.

Assume that $E_s = 1$, $E_p = 1$, $c_d = 1$, $\varepsilon_0 = 0$, $t_1 = 1$, and $t_2 = 2$.

Solution

Table 2.7 lists the solutions of the constitutive equations of Maxwell and Kelvin–Voigt models for the given loading and unloading cycle.

Figure 2.8a,b displays the stress–strain characteristics of the Maxwell and Kelvin–Voigt models. The figures indicate that, according to the Maxwell model, the VEM is stiffer and dissipates less energy, as represented by the enclosed area, than that predicted by the Kelvin–Voigt model.

2.3 Creep Compliance and Relaxation Modulus

In Section 2.2, time domain relationships are derived for the different classical VEM models when these models are subjected to creep or relaxation loading. These relationships are obtained by solving the constitutive equations that describe the dynamics of the VEM models subject to initial conditions determined by applying the initial value theorem.

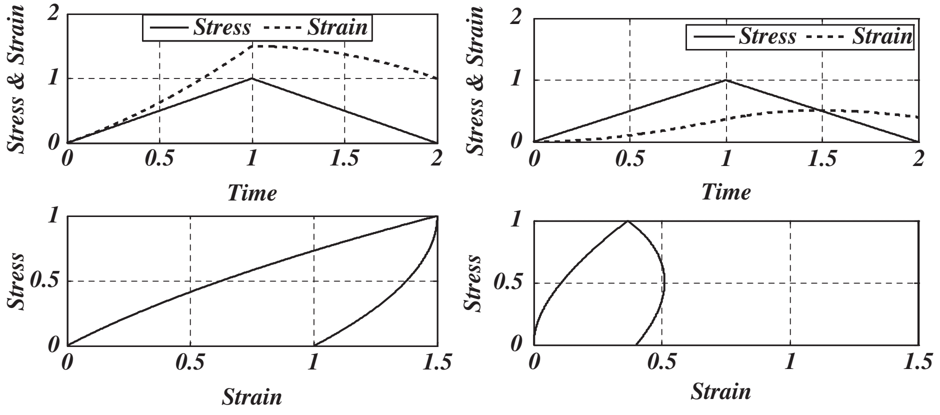

(a) – Maxwell model

(b) – Kelvin-Voigt model

Figure 2.8 Stress–strain characteristics of Maxwell and Kelvin–Voigt models. (a) Maxwell model and (b) Kelvin–Voigt model.

Table 2.8 lists these relationships such that the ratio between the strain and amplitude of the creep stress ε/σ_0 is denoted by the symbol *J(t)* and called "the creep compliance" and the ratio between the stress and amplitude of the relaxation strain σ/ε_0 is designated by the symbol $E(t)$ and called "the relaxation modulus."

It is important to note that these two characteristic properties of VEM are time-dependent, unlike the corresponding properties for solids, which are constants.

Note also that the process involved in deriving these properties has been tedious and cumbersome as it consists of applying the initial and final value theorems followed by the exhaustive procedure for solving the constitutive equations subject to the initial values and then validating the solution against the obtained final values.

In this section, two other approaches are presented. In the first approach, the direct Laplace and inverse Laplace transformations are applied one after the other to the constitutive equations of the VEM. In the second approach, the topology of the VEM model is translated into a linear set of equations that can be reduced by using the Gauss elimination to determine both $J(t)$ and $E(t)$ simultaneously. The two approaches are implemented in a MATLAB environment to enhance their practicality and utility.

Table 2.8 The creep characteristics of Maxwell, Kelvin–Voigt, and Poynting–Thomson models.

Model	Maxwell model	Kelvin–Voigt model	Poynting–Thomson model
Creep compliance (J)	$J=\frac{\varepsilon}{\sigma_0}=\frac{1}{E_s}\left(1+\frac{t}{\lambda}\right)$[a]	$J=\frac{\varepsilon}{\sigma_0}=\frac{1}{E_s}\left[1-e^{-t/\lambda}\right]$[a]	$J=\frac{\varepsilon}{\sigma_0}=\frac{1}{E_\infty}\left[1+\frac{E_\infty-E_s}{E_s}e^{-t/\lambda}\right]$
Relaxation modulus (E)	$E=\frac{\sigma}{\varepsilon_0}=E_s e^{-t/\lambda}$	$E=\frac{\sigma}{\varepsilon_0}=E_s+c_d\,dirac(t)$[b] $=\frac{\sigma}{\varepsilon_{0+}}=E_s$	$E=\frac{\sigma}{\varepsilon_0}=E_\infty\left(1-e^{-t/\alpha}\right)+E_s e^{-t/\alpha}$ where $\alpha=\frac{c_d}{\left(E_s+E_p\right)}$, $\lambda=\frac{c_d}{E_p}$

[a] $\lambda = c_d/E_s$.

[b] $dirac(t) = \infty$ at $t = 0$ and 0 at $t = 0+$.

2.3.1 Direct Laplace Transformation Approach

The constitutive equations of the VEM are transformed into the Laplace domain to assume one of the following transfer function forms:

$$J^* = \frac{\varepsilon}{\sigma} \tag{2.26a}$$

and

$$E^* = \frac{\sigma}{\varepsilon} \tag{2.26b}$$

When the VEM is subjected to creep loading, the stress σ is replaced by its Laplace transform σ_0/s and Eq. (2.26a) reduces to:

$$J^* = s\frac{\varepsilon}{\sigma_0} = sJ(s) \tag{2.27a}$$

Similarly, when the VEM is subjected to relaxation loading, the strain ε is replaced by its Laplace transform ε_0/s and Eq. (2.26b) reduces to:

$$E^* = s\frac{\sigma}{\varepsilon_0} = sE(s) \tag{2.27b}$$

The inverse Laplace transform is then used to transform $J(s)$ and $E(s)$ into the time domain creep compliance $J(t)$ and relaxation modulus $E(t)$.

Table 2.9 lists the corresponding creep compliance $J(t)$ and relaxation modulus $E(t)$ for the Maxwell, Kelvin–Voigt, and Poynting–Thomson models.

Table 2.9 Time domain characteristics of classical viscoelastic models.

Operation	Maxwell	Kelvin–Voigt	Poynting–Thomson
Dynamic equations	$\lambda\dot{\sigma} + \sigma = c_d\dot{\varepsilon}$	$\sigma = E_s\varepsilon + c_d\dot{\varepsilon}$	$(E_s + E_p)\sigma + c_d\dot{\sigma}$ $= E_sE_p\varepsilon + E_sc_d\dot{\varepsilon}$
Laplace transform of the strain due to creep loading $\boldsymbol{\sigma_0}$	$\frac{\varepsilon}{\sigma_0} = \frac{\lambda s + 1}{c_d s^2}$	$\frac{\varepsilon}{\sigma_0} = \frac{1}{E_s s(\lambda s + 1)}$	$\frac{\varepsilon}{\sigma_0} = \frac{(E_s + E_p) + c_d s}{(E_sE_p + E_sc_d s)s}$
Inverse Laplace transform of $\boldsymbol{\varepsilon/\sigma_0 = J}$ **using MATLAB**	>> **syms** L cd s t >> **ilaplace** ((L*s + 1)/(cd*s^2),s,t) **J** = λ/cd + t/cd	>> **syms** L E s t >> **ilaplace**(1/(E*s*(L*s + 1)),s,t) **J** = 1/E – 1/(E* exp(t/λ))	>> **syms** Es Ep cd s t >> **ilaplace** (((Es + Ep) + cd*s)/(s*(Es*Ep+Es*cd*s)),s,t) **J** = (Ep + Es)/(Ep*Es) - 1/(Ep*exp((Ep*t)/cd))
Laplace transform of the stress due to relaxation loading $\boldsymbol{\varepsilon_0}$	$\frac{\sigma}{\varepsilon_0} = \frac{c_d}{\lambda s + 1}$	$\frac{\sigma}{\varepsilon_0} = \frac{E_s(\lambda s + 1)}{s}$	$\frac{\sigma}{\varepsilon_0} = \frac{(E_sE_p + E_sc_d s)}{[(E_s + E_p) + c_d s]s}$
Inverse Laplace transform of $\boldsymbol{\sigma/\varepsilon_0 = R}$ **using MATLAB**	>> **syms** L cd s t >> **ilaplace** ((cd)/(L*s+1),s,t) R = cd/(λ* exp(t/λ))	>> **syms** L E s t >> **ilaplace**(E*(L*s + 1)/s,s,t) **R** = E + E*L*dirac(t)	>> **syms** Es Ep cd s t >> **ilaplace**((Es*Ep + Es*cd*s)/(s*(Es + Ep + cd*s)),s,t) **R** = (Ep*Es)/(Ep + Es) + Es^2/(exp((t*(Ep + Es))/cd)*(Ep + Es))

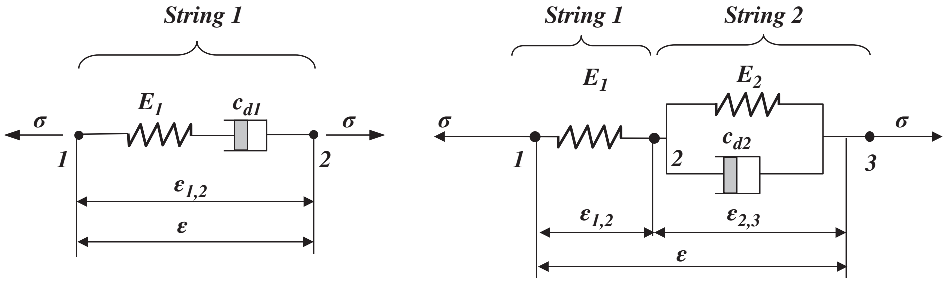

(a) – Maxwell model (b) – Poynting-Thomson Model

Figure 2.9 Topology of the Maxwell and Poynting–Thomson models. (a) Maxwell model and (b) Poynting–Thomson model.

2.3.2 Approach of Simultaneous Solution of a Linear Set of Equilibrium, Kinematic, and Constitutive Equations

This approach was developed by Vondřejc (2009) and translates the topology of the VEM model into a linear set of equilibrium, kinematic, and constitutive equations which can be reduced by using the Gauss elimination to determine both J and R simultaneously. The approach is implemented in a MATLAB environment to enhance its practicality and utility.

In this approach, the topology of the viscoelastic model is described by N serial strings extending between P points. Each string can consist of a spring and a damper in series. For example, Figure 2.9 shows the description of the topology of the Maxwell and Poynting–Thomson VEM models. In Figure 2.9a, the Maxwell model is described by one string and two points whereas in Figure 2.9b, the Poynting–Thomson model is defined by two strings and three points.

In a symbolic MATLAB environment, the topology description of the two models is given by the vectors B such that:

Maxwell Model: B = [1, 2, E_1, cd_1],

Poynting–Thomson Model: B = [1, 2, E_1, *inf*; 2, 3, E_2, *inf*; 2, 3, *inf*, cd_2];

Note that in this description of any string, the component value of a spring or a damper that is missing in the string is set equal to "inf."

The mathematical formulation of the *VEM* model, in the Laplace domain, is described as follows:

Constitutive equations

$$-\sum_{j=b_i}^{e_i-1}\varepsilon_{j,j+1}+\sigma_i\left(\frac{1}{E_i}+\frac{1}{c_{d_i}s}\right)=0 \quad i=1,2,\ldots,N \tag{2.28}$$

Equilibrium equations

$$-\sum_{j=1}^{P}\delta_{ib_j}\sigma_j+\sigma=0 \qquad \text{For beginning points } b_j \tag{2.29}$$

$$\sum_{j=1}^{P}\left(\delta_{ib_j}-\delta_{ie_j}\right)\sigma_j=0 \quad i=1,2,\ldots,P-1 \tag{2.30}$$

$$-\sum_{k=1}^{P}\delta_{ie_k}\sigma_k+\sigma=0 \qquad \text{For end points } e_k \tag{2.31}$$

Kinematic equations

$$-\sum_{j=1}^{P-1}\varepsilon_{j,j+1}+\varepsilon=0 \tag{2.32}$$

Note that b_j and e_j denote the beginning and end points of the jth string.
In a matrix form, Eqs. (2.28) through (2.32) take the following form:

$$Ax = 0 \tag{2.33}$$

where x is a vector of the strains and stresses given by:

$$x = \{\varepsilon_{1,2} \;\; \varepsilon_{2,3} \ldots \varepsilon_{P-1,P} \;\; \sigma_1 \; \sigma_2 \ldots \sigma_N \;\; \sigma \;\; \varepsilon\} \tag{2.34}$$

where $\varepsilon_{j,\,j+1}$ = strain between points j and $j+1$, σ_i = stress in the ith string, σ = stress applied to the entire VEM topology, and ε = total strain of the entire VEM topology.

Example 2.2 Derive expressions for the creep compliance and relaxation modulus for the Maxwell model using the approach of simultaneous solution of a linear set of equilibrium, kinematic, and constitutive equations described in Section 2.3.2.

Solution

From Eqs. (2.28) through (2.32), the system of equations describing the dynamics of the Maxwell model is given by:

$$\begin{bmatrix} -1 & C & 0 & 0 \\ 0 & -1 & 1 & 0 \\ 0 & -1 & 1 & 0 \\ -1 & 0 & 0 & 1 \end{bmatrix} \begin{Bmatrix} \varepsilon_{1,2} \\ \sigma_{1,2} \\ \sigma \\ \varepsilon \end{Bmatrix} = 0 \quad \text{or} \quad Ax = 0 \tag{2.35}$$

where $C = \dfrac{1}{E_1} + \dfrac{1}{c_{d1}s}$.

Applying the Gauss elimination method to Eq. (2.35), it reduces to:

$$\begin{bmatrix} -1 & C & 0 & 0 \\ 0 & -1 & 1 & 0 \\ 0 & 0 & 0 & 0 \\ 0 & 0 & -C & 1 \end{bmatrix} \begin{Bmatrix} \varepsilon_{1,2} \\ \sigma_{1,2} \\ \sigma \\ \varepsilon \end{Bmatrix} = 0 \tag{2.36}$$

Expanding the last row of Eq. (2.36) gives:

$$C\sigma = \varepsilon \quad \text{or} \quad \left(\frac{1}{E_1} + \frac{1}{c_{d1}s}\right)\sigma = \varepsilon \tag{2.37}$$

Hence, if the VEM is subjected to creep loading such that $\sigma = \sigma_0$, then Eq. (2.37) reduces to:

$$\varepsilon = \left[\frac{1}{E_1} + \frac{1}{c_{d1}s}\right]\frac{\sigma_0}{s} \tag{2.38}$$

Using MATLAB symbolic manipulation gives:

```
>> syms E1 cd1 sigma0 s t
>> ilaplace ((1/E1+1/(cd1*s))*sigma0/s, s, t)
J = sigma0/E1 + (sigma0*t)/cd1)
```

Note that the obtained creep compliance J matches that listed in Table 2.9.

Also, if the VEM is subjected to relaxation strain such that $\varepsilon = \varepsilon_0$, then Eq. (2.37) reduces to:

$$\sigma = \frac{\varepsilon_0}{s} \Big/ \left[\frac{1}{E_1} + \frac{1}{c_{d1}s}\right] \tag{2.39}$$

Using MATLAB symbolic manipulation gives:

```
>> syms E1 cd1 eps0 s t
>> ilaplace (1/(1/E1+1/(cd1*s))*eps0/s, s, t)
E = (E1*eps0)/exp((E1*t)/cd1)
```

The obtained relaxation modulus E matches that listed in Table 2.9.

2.4 Characteristics of the VEM in the Frequency Domain

Assume a VEM is subjected to sinusoidal stress σ and strain ε, at a frequency ω, such that:

$$\sigma = \sigma_0 e^{i\omega t} \text{ and } \varepsilon = \varepsilon_0 e^{i\omega t} \tag{2.40}$$

where σ_0 and ε_0 denote the amplitude of the stress and strain, respectively, with $i = \sqrt{-1}$.

Hence, for a VEM described by the Maxwell model, Eqs. (2.9) and (2.26b) give:

$$(1 + i\lambda\omega)\sigma_0 e^{i\omega t} = \lambda E_s \omega \varepsilon_0 i\, e^{i\omega t} \quad \text{or} \quad \sigma_0 = E_s \left[\frac{\omega^2\lambda^2}{1+\omega^2\lambda^2} + i\frac{\omega\lambda}{1+\omega^2\lambda^2}\right]\varepsilon_0.$$

In a compact form,

$$\sigma_0 = E'[1 + i\eta]\,\varepsilon_0 \tag{2.41}$$

where $E' = E_s\left[\frac{\omega^2\lambda^2}{1+\omega^2\lambda^2}\right]$ and $\eta = \frac{1}{\omega\lambda}$. The constitutive equation of the VEM, as given by Eq. (2.41), indicates that the material has a complex modulus $E^* = E'[1 + j\eta]$ that relates the stress and the strain. Note that:

a) the real part of the complex modulus = E' is called the *storage modulus*,
b) the imaginary part of the modulus = $E'\eta$ is called the *loss modulus* E'', and
c) the ratio between loss and the storage moduli is η is called the *loss factor*.

Figure 2.10 shows the effect of the excitation frequency on the storage modulus and the loss factor of the Maxwell model.

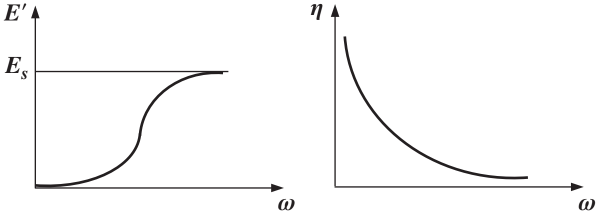

(a) – Storage Modulus (b) – Loss Factor

Figure 2.10 Effect of frequency on the storage modulus and loss factor of Maxwell model. (a) Storage modulus and (b) loss factor.

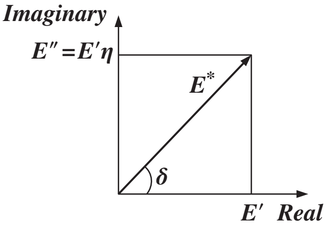

Figure 2.11 Graphical representation of complex modulus.

Note that the Maxwell model indicates that the VEM has zero storage modulus under static conditions ($\omega = 0$) and has a loss factor that is continuously decaying with frequency. These two characteristics contradict the behavior of realistic VEMs.

Figure 2.11 displays graphically the different components of the complex modulus $E^* = E'[1 + i\,\eta]$.

Note that the complex modulus makes an angle δ with the real axis such that:

$$\tan(\delta) = \eta \tag{2.42}$$

Because of this relationship, the loss factor is also called “tan delta” or the “loss tangent.”

In a similar manner, the constitutive equations for the Kelvin–Voigt and Poynting–Thomson models can be determined in the frequency domain. Table 2.10 lists these equations and gives expressions for the corresponding storage modulus and loss factor for the different models.

The characteristics summarized in Table 2.10 ascertain the ability of the Poynting–Thomson model to simulate a realistic behavior of VEMs. However, several

Table 2.10 Frequency domain characteristics of classical viscoelastic models.

Parameter	**Maxwell**	**Kelvin–Voigt**	**Poynting–Thomson**
Model	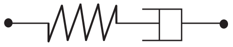	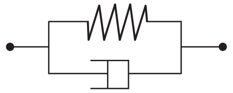	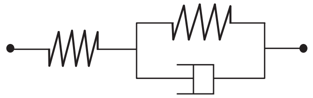
Storage modulus	$E' = E_s\left[\dfrac{\omega^2\lambda^2}{1+\omega^2\lambda^2}\right]$	$E' = E_s$	$E' = E_\infty\left[\dfrac{1+\alpha\beta\omega^2}{1+\alpha^2\omega^2}\right]$[a]
	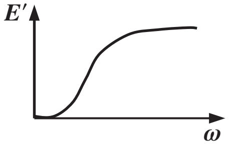	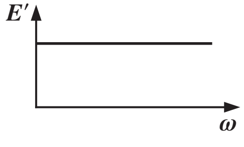	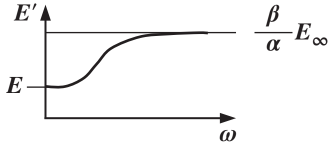
Comments	Unrealistic	Unrealistic	Realistic
Loss Factor	$\eta = 1/\omega\lambda$	$\eta = \omega\lambda$	$\eta = (\beta - \alpha)\omega/[1 + \alpha\beta\omega^2]$
	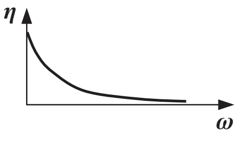	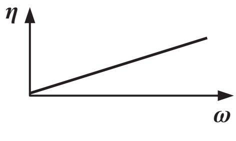	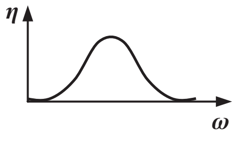
Comments	Unrealistic	Unrealistic	Realistic

[a] where $E_\infty = \dfrac{E_s E_p}{E_s + E_p}$, $\alpha = \dfrac{c_d}{E_s + E_p}$, and $\beta = \dfrac{c_d}{E_p}$.

combinations of Poynting–Thomson models are necessary to replicate the behavior of realistic VEMs.

2.5 Hysteresis and Energy Dissipation Characteristics of Viscoelastic Materials

2.5.1 Hysteresis Characteristics

Consider a VEM subjected to sinusoidal stress σ and strain ε given by

$$\sigma = \sigma_0 e^{i\omega t} \text{ and } \varepsilon = \varepsilon_0 e^{i\omega t} \tag{2.43}$$

with the stress and strain related by the following constitutive equation

$$\sigma = E'(1 + i\eta)\,\varepsilon \tag{2.44}$$

Combining Eqs. (2.43) and (2.44) gives

$$\begin{aligned}\sigma &= \sigma_0 \sin(\omega t)\\ &= E'\varepsilon_0 \sin(\omega t) + \eta E'\varepsilon_0 \cos(\omega t)\\ &= \sigma_e + \sigma_d\end{aligned} \tag{2.45}$$

where $\sigma_e = E'\varepsilon_0 \sin(\omega t)$ and $\sigma_d = \eta E'\varepsilon_0 \cos(\omega t)$ denote the elastic and dissipative components of the applied stress σ.

Then σ_d can be written as:

$$\begin{aligned}\sigma_d &= \eta E'\varepsilon_0 \cos(\omega t)\\ &= \pm\,\eta E'\sqrt{\varepsilon_0^2 - \varepsilon_0^2 \sin^2(\omega t)}\\ &= \pm\,\eta E'\sqrt{\varepsilon_0^2 - \varepsilon^2}\end{aligned} \tag{2.46}$$

Rearranging this equation reduces it to

$$(\sigma_d/\eta E')^2 + \varepsilon^2 = \varepsilon_0^2 \tag{2.47}$$

which is an equation of an ellipse as shown in Figure 2.12a. Figure 2.12b shows a plot of the elastic stress versus the strain and Figure 2.12c combines the elastic and dissipative stress components. Figure 2.12c displays accordingly the total stress σ acting on the VEM versus the strain ε.

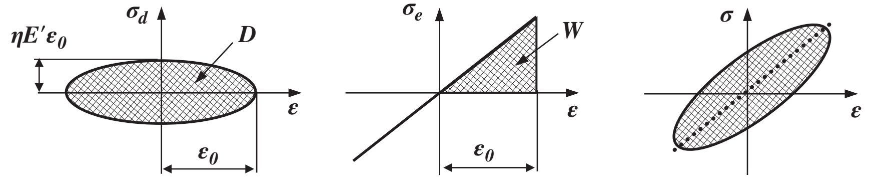

(a) – dissipative component (b) – elastic component (c) – viscoelastic material

Figure 2.12 Stress–strain relationship for a viscoelastic material. (a) dissipative component, (b) elastic component, and (c) viscoelastic material.

Note that the dissipative component takes the form of a hysteresis loop. The area inside the loop quantifies the amount of energy D dissipated during the cyclic deformation of the VEM.

2.5.2 Energy Dissipation

The energy dissipated during a full vibration cycle of the VEM, at a frequency ω, per unit volume can be determined from

$$D = \int \sigma_d d\varepsilon = \int_0^{\frac{2\pi}{\omega}} \sigma_d \frac{d\varepsilon}{dt} dt \tag{2.48}$$

But as $\sigma_d = \eta E' \varepsilon_0 \cos(\omega t)$ and $\varepsilon = \varepsilon_0 \sin(\omega t)$, then Eq. (2.48) reduces to

$$\begin{aligned} D &= \int_0^{\frac{2\pi}{\omega}} \sigma_d \frac{d\varepsilon}{dt} dt \\ &= \int_0^{\frac{2\pi}{\omega}} [\eta E' \varepsilon_0 \cos(\omega t)]\,[\omega \varepsilon_0 \cos(\omega t)] dt \\ &= \pi \eta E' \varepsilon_0^2 \end{aligned} \tag{2.49}$$

2.5.3 Loss Factor

Two methods can be used to extract the loss factor from the hysteresis characteristics of the VEM. These methods are based on the following:

2.5.3.1 Relationship Between Dissipation and Stored Elastic Energies

Consider now the energy W stored in the elastic component, during one-quarter of a vibration cycle, which can be determined from:

$$W = \int \sigma_e d\varepsilon = \int_0^{\frac{\pi}{2\omega}} \sigma_e \frac{d\varepsilon}{dt} dt$$

With $\sigma_e = E' \varepsilon_0 \sin(\omega t)$, the equation reduces to

$$\begin{aligned} W &= \int_0^{\frac{\pi}{2\omega}} \sigma_e \frac{d\varepsilon}{dt} dt \\ &= \int_0^{\frac{\pi}{2\omega}} [E' \varepsilon_0 \sin(\omega t)]\,[\omega \varepsilon_0 \cos(\omega t)]\, dt \\ &= \frac{1}{2} E' \varepsilon_0^2 \end{aligned} \tag{2.50}$$

From Eqs. (2.49) and (2.50), the loss factor η can be determined from

$$\eta = \frac{D}{2\pi W} \tag{2.51}$$

Hence, Eq. (2.51) defines the physical meaning of the loss factor as the ratio between the dissipated energy and stored energy. Also, Figure 2.12 shows the graphical representation and physical meaning of both the dissipated and stored energies.

2.5.3.2 Relationship Between Different Strains

Equations (2.45) and (2.46) can be rewritten as:

$$\sigma = E'\varepsilon \pm \eta E' \sqrt{\varepsilon_0^2 - \varepsilon^2} \tag{2.52}$$

When the stress σ is set = 0, the corresponding strain ε_{sf} can be obtained from:

$$0 = E'\varepsilon_{sf} \pm \eta E' \sqrt{\varepsilon_0^2 - \varepsilon_{sf}^2}$$

or,

$$\varepsilon_{sf} = \frac{\eta}{\sqrt{1+\eta^2}}\varepsilon_0 \tag{2.53}$$

The $\sigma - \varepsilon$ relationship of the upper branch of hysteresis characteristics can be expressed form Eq. (2.45) as:

$$\sigma = E'\varepsilon + \eta E' \sqrt{\varepsilon_0^2 - \varepsilon^2} \tag{2.54}$$

The maximum stress is attained when:
$\frac{d\sigma}{d\varepsilon} = 0$ at $\varepsilon = \varepsilon_{\max\sigma}$ given by:

$$\varepsilon_{\max\sigma} = \varepsilon_0 / \sqrt{1+\eta^2} \tag{2.55}$$

Figure 2.13 displays the graphical interpretation of the strains ε_{sf} and $\varepsilon_{\max\sigma}$.
From Eqs. (2.53) and (2.55),

$$\frac{\varepsilon_{sf}}{\varepsilon_{\max\sigma}} = \eta \tag{2.56}$$

Hence, the loss factor can be computed as the ratio between the two strains ε_{sf} and $\varepsilon_{\max\sigma}$ as measured from the hysteresis characteristics.

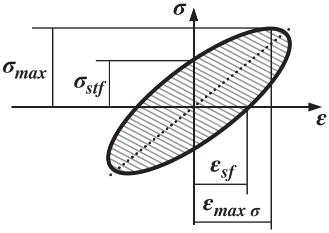

Figure 2.13 Graphical representation of the strains ε_{sf} and $\varepsilon_{\max\sigma}$.

2.5.4 Storage Modulus

The storage modulus can be determined by considering the stress under a strain-free condition σ_{stf}. This value can be obtained by setting $\varepsilon = 0$ in Eq. (2.54), giving:

$$\sigma_{stf} = \pm \eta E' \varepsilon_0 \tag{2.57}$$

Once η and ε_0 are determined from Eqs. (2.56) and (2.53), then Eq. (2.57) can be used to compute the storage modulus E'.

Example 2.3 Plot the stress–strain characteristics for the Poynting–Thomson model when the VEM is subjected to sinusoidal stress such that $\sigma = \sin t$. Assume that $E_s = 1$, $E_p = 1$, and $c_d = 1$. Determine the loss factor and the storage modulus according to the methods described in Sections 2.5.3.2 and 2.5.4. Compare the results with the loss factor and the storage modulus expressions listed in Table 2.10.

Solution

The constitutive equation for the Poynting–Thomson model is:

$$\dot{\varepsilon} + \varepsilon = \dot{\sigma} + 2\sigma$$

For sinusoidal stress: $\sigma = \sin t$, this equation reduces to:

$$\dot{\varepsilon} + \varepsilon = 2\sin t + \cos t$$

This equation is integrated numerically, with respect to time, using MATLAB to extract the time history of the strain as function of the time history of the input stress. Then, the strain is plotted against the stress to yield the stress–strain characteristics shown in Figure 2.14.

a) From Figure 2.14,

$$\varepsilon_{\max\sigma} = \varepsilon_0 / \sqrt{1+\eta^2} = 1.5$$

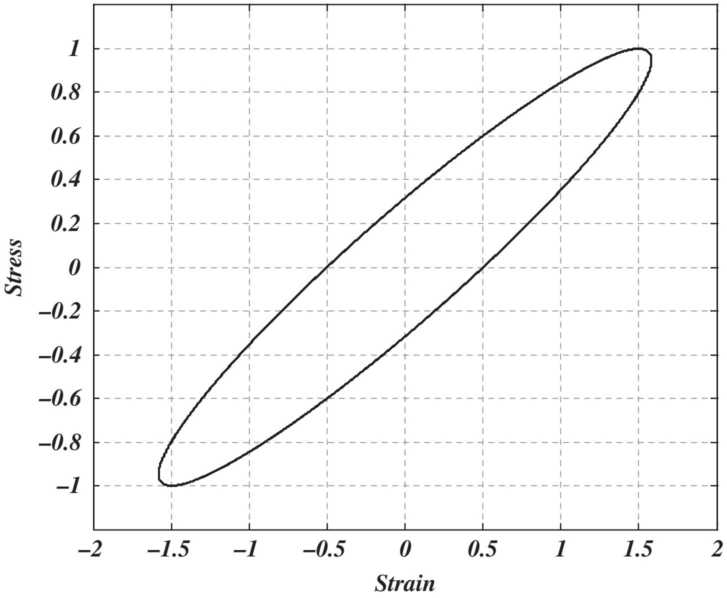

Figure 2.14 Stress–strain characteristics of a Poynting–Thomson model.

$$\varepsilon_{sf} = \frac{\eta}{\sqrt{1+\eta^2}}\varepsilon_0 = 0.5$$

Then,

$$\frac{\varepsilon_{sf}}{\varepsilon_{\max\sigma}} = \eta = \frac{0.5}{1.5} = 0.33$$

This yields $\varepsilon_0 = 1.581$.

Also, from Figure 2.14, $\sigma_{stf} = \pm\eta E'\varepsilon_0 = \pm 0.3148$, or

$$E' = 0.3148/(\eta\varepsilon_0)$$
$$= 0.3148/(0.333 \times 1.581) = 0.598$$

b) From Table 2.10,

$$\text{As}\, E = \frac{E_s E_p}{E_s + E_p} = \frac{1}{2},\ \alpha = \frac{c_d}{E_s + E_p} = \frac{1}{2},\ \beta = \frac{c_d}{E_p} = 1,\ \text{ and }\ \omega = 1.$$

Then,

$$E' = E\left[\frac{1+\alpha\beta\omega^2}{1+\alpha^2\omega^2}\right] = \frac{1}{2}\left[\frac{1+0.5\omega^2}{1+0.25\omega^2}\right] = \frac{1.5}{2\times 1.25} = 0.6$$

and

$$\eta = (\beta-\alpha)\omega/\left[1+\alpha\beta\omega^2\right] = 0.5/(1+0.5) = 0.333$$

Hence, the two methods yield exactly the same results.

Example 2.4 Plot the storage modulus and the loss factor as predicted by a Maxwell, Kelvin–Voigt, and Poynting–Thomson models that best fits the experimental behavior of the VEM Dyad 606 (Soundcoat, Deer Park, NY) at 37.8°C (100°F).

Solution

The storage modulus and the loss factor of the different VEM models, listed in Table 2.10, are plotted versus the frequency ω as shown in Figure 2.15. The plots are obtained for $\alpha = 1$, $\beta = 20$, $\lambda = 3$, $E_s = 500$, and $E = 500$.

The figure indicates clearly that all the three models are incapable of capturing the behavior of the Dyad606. However, the predictions of the Poynting–Thomson model qualitatively have the general trends but fail to quantitatively describe the behavior over a broad frequency range.

A combination of several Poynting–Thomson models is necessary to replicate the behavior of realistic VEMs.

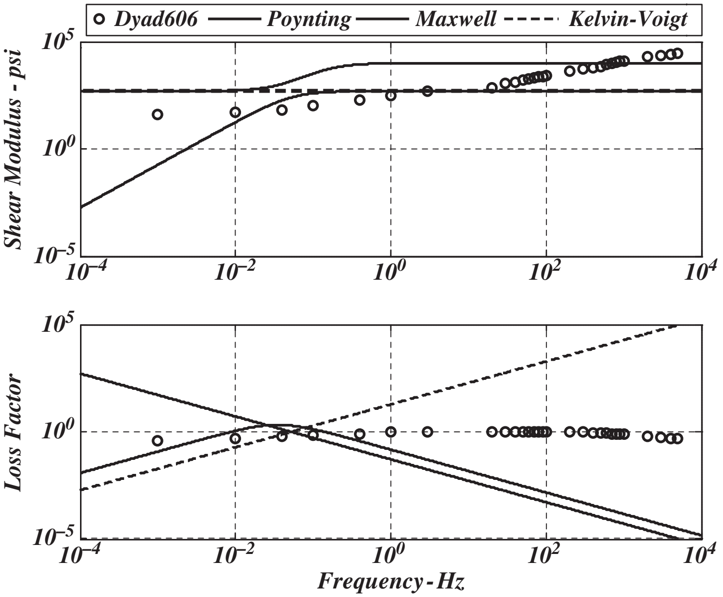

Figure 2.15 Storage modulus and loss factor of different VEM models.

2.6 Fractional Derivative Models of Viscoelastic Materials

As indicated in Section 2.5, the simple classical models of VEMs cannot replicate the dynamic behavior of real VEMs. Other alternative models have been considered to overcome such serious limitations. Among these models are fractional derivative (FD) model (Bagley and Torvik 1983), Golla–Hughes–MacTavish (GHM) model (Golla and Hughes 1985), and the Augmented Temperature Field model (Lesieutre and Mingori 1990; Lesieutre et al. 1996).

2.6.1 Basic Building Block of Fractional Derivative Models

The basic concepts of fractional calculus are summarized in Appendix 2.B.

In this section, the basic building block of FD models is the “spring-pot” that replaces the spring and dashpot elements used in the classical models. The spring-pot element is employed to simplify, improve the applicability, and reduce the number of parameters used to model the complex behavior of viscoelastic polymers.

The spring-pot element is a nonlinear FD element that has the following constitutive equation:

$$\sigma(t) = E\tau^{\alpha}\frac{d^{\alpha}\varepsilon(t)}{dt^{\alpha}} \tag{2.58}$$

Note that the stress $\sigma(t)$ applied to the element is dependent on the FD of order α of the strain $\varepsilon(t)$ where α ranging between 0 and 1. When α = 0, the spring-pot element reduces to a linear spring and when α = 1, the spring-pot element becomes a linear dashpot (damper) as shown in Figure 2.16.

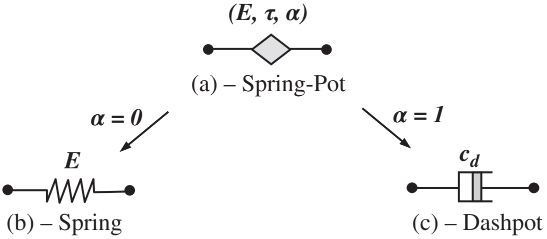

Figure 2.16 Representations of a spring-pot, spring, and dashpot. (a) Spring-pot, (b) spring, and (c) dashpot.

From Eq. (2.58), the storage and loss moduli of the spring-pot can be determined as follows:

$$\begin{aligned} E^*(\omega) &= E\,(i\omega\tau)^{\alpha} \\ &= E\,(\omega\tau)^{\alpha}\, e^{\frac{\pi}{2}\alpha i} \\ &= E\,(\omega\tau)^{\alpha}\left[\cos\left(\frac{\pi}{2}\alpha\right) + i\sin\left(\frac{\pi}{2}\alpha\right)\right] \\ &= E' + iE'' \end{aligned} \tag{2.59}$$

where $E' = E\,(\omega\tau)^{\alpha}\cos\left(\frac{\pi}{2}\alpha\right)$ and $E'' = E\,(\omega\tau)^{\alpha}\sin\left(\frac{\pi}{2}\alpha\right)$.

The relaxation modulus $E(t)$ of the spring-pot can be obtained by applying the inverse Fourier transform to Eq. (2.58) knowing that $E(s) = E^*/s$, as indicated in Eq. (2.27b). This yields the following expressions:

Relaxation modulus

$$\begin{aligned} E(t) &= \frac{2}{\pi}\int_0^{\infty}\left[\frac{1}{\omega}E'\sin(\omega t)\right]d\omega \\ &= \frac{2}{\pi}E\,\tau^{\alpha}\cos\left(\frac{\pi}{2}\alpha\right)\int_0^{\infty}\left[\omega^{\alpha-1}\sin(\omega t)\right]d\omega \\ &= \frac{E}{\Gamma(1-\alpha)}\left(\frac{t}{\tau}\right)^{-\alpha} \end{aligned} \tag{2.60}$$

and

Creep compliance

$$J(t) = \frac{E^{-1}}{\Gamma(1+\alpha)}\left(\frac{t}{\tau}\right)^{\alpha} \tag{2.61}$$

2.6.2 Basic Fractional Derivative Models

The basic FD models presented in this section are the FD Maxwell, FD Kelvin–Voigt, and FD Poynting–Thomson models.

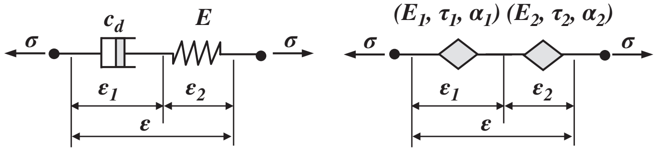

(a) (b)

Figure 2.17 Classical (a) and fractional derivative (b) Maxwell models.

For example, consider the classical Maxwell model shown in Figure 2.17a is transformed to a FD Maxwell model shown in Figure 2.17b by replacing each component by a spring-pot with different parameters.

For the FD model and using the equivalent spring-pot Eq. (2.58), the strains ε_1 and ε_2 can be written as:

$$\varepsilon_1(t) = E_1^{-1}\tau_1{}^{-\alpha_1}\frac{d^{-\alpha_1}\sigma(t)}{dt^{-\alpha_1}} \text{ and } \varepsilon_2(t) = E_2^{-1}\tau^{-\alpha_2}\frac{d^{-\alpha_2}\sigma(t)}{dt^{-\alpha_2}} \tag{2.62}$$

But as, $\varepsilon = \varepsilon_1 + \varepsilon_2$, then:

$$\sigma(t) + \tau^{\alpha_1-\alpha_2}\frac{d^{\alpha_1-\alpha_2}\sigma(t)}{dt^{\alpha_1-\alpha_2}} = E\tau^{\alpha_1}\frac{d^{\alpha_1}\varepsilon(t)}{dt^{\alpha_1}} \tag{2.63}$$

where $\tau = (E_1\tau_1^{\alpha_1}/E_2\tau_2^{\alpha_2})^{1/(\alpha_1-\alpha_2)}$, $E = E_1(\tau_1/\tau_2)^{\alpha_1}$, and $\alpha_1 \geq \alpha_2$.

Fourier-transforming Eq. (2.63) gives:

$$E^* = \frac{E(i\omega\tau)^{\alpha_1}}{1 + (i\omega\tau)^{\alpha_1-\alpha_2}} \tag{2.64}$$

Following the same approach adopted in Section 2.6.1, it can be easily shown that the relaxation modulus and creep compliance of the FD Maxwell model are given by:

$$J(t) = \frac{E^{-1}}{\Gamma(1+\alpha_1)}\left(\frac{t}{\tau}\right)^{\alpha_1} + \frac{E^{-1}}{\Gamma(1+\alpha_2)}\left(\frac{t}{\tau}\right)^{\alpha_2} \tag{2.65}$$

Table 2.11 summarizes the complex moduli for the FD Maxwell, Kelvin–Voigt, and Zener models.

Example 2.5 Determine the storage modulus, loss modulus, and loss factor as predicted by the FD Zener model that is given by the following four-parameter FD model proposed by Bagley and Torvik (1983):

$$\sigma(t) + \tau^{\alpha}D^{\alpha}\sigma(t) = E_0\varepsilon(t) + E_{\infty}\tau^{\alpha}D^{\alpha}\varepsilon(t)$$

where $E_0 = E_sE_p/(E_s + E_p)$ = relaxed elastic modulus, $E_\infty = E_s$ = unrelaxed elastic modulus, $\tau = c_d/(E_s + E_p)$ = the relaxation time, and $0 < \alpha < 1$.

Solution

From Eq. (2.58), the complex modulus as predicted by the four-parameter FD model can be obtained by using Eq. (2.B.10), to give:

$$E^* = \frac{\sigma(s)}{\varepsilon(s)} = \frac{E_0 + E_\infty(\tau s)^\alpha}{1 + (\tau s)^\alpha}$$

Table 2.11 Frequency domain characteristics of fractional derivative viscoelastic models.

Parameter	Maxwell	Kelvin–Voigt	Zener
Model	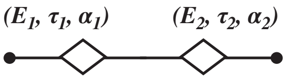	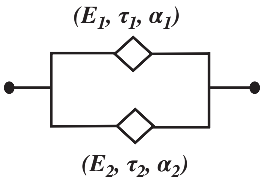	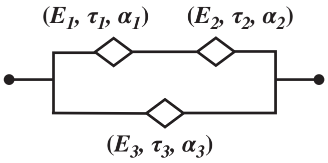
Storage modulus	$E^* = \frac{E(i\omega\tau)^{\alpha_1}}{1+(i\omega\tau)^{\alpha_1-\alpha_2}}$[a]	$E^* = E(i\omega\tau)^{\alpha_1} + E(i\omega\tau)^{\alpha_2}$	$E^* = E_0\frac{(i\omega\tau)^{\alpha_2}}{1+(i\omega\tau)^{\alpha_2-\alpha_1}} + E(i\omega\tau)^{\alpha_3}$[b]

[a] where $\tau = (E_1\tau_1^{\alpha_1}/E_2\tau_2^{\alpha_2})^{1/(\alpha_1-\alpha_2)}$, $E = E_1(\tau_1/\tau_2)^{\alpha_1}$, and $\alpha_1 \geq \alpha_2$.
[b] $E_0 = E_1(\tau_1/\tau)^{\alpha_1}$.

It can be easily shown that the storage and loss moduli of the four-parameter FD model are given by:

$$E'(\omega) = \frac{E_0 + (E_\infty + E_0)(\omega\tau)^\alpha \cos(\pi\alpha/2) + E_\infty(\omega\tau)^{2\alpha}}{1 + 2(\omega\tau)^\alpha \cos(\pi\alpha/2) + (\omega\tau)^{2\alpha}}$$

and

$$E''(\omega) = \frac{(E_\infty - E_0)(\omega\tau)^\alpha \sin(\pi\alpha/2)}{1 + 2(\omega\tau)^\alpha \cos(\pi\alpha/2) + (\omega\tau)^{2\alpha}}$$

Accordingly, the loss factor η is given by:

$$\eta = \frac{E''(\omega)}{E'(\omega)} = \frac{(E_\infty - E_0)(\omega\tau)^\alpha \sin(\pi\alpha/2)}{E_0 + (E_\infty + E_0)(\omega\tau)^\alpha \cos(\pi\alpha/2) + E_\infty(\omega\tau)^{2\alpha}}$$

This yields a value of α that can be estimated from (see Problem 2.9):

$$\alpha = \frac{2}{\pi}\sin^{-1}\left[\eta_{\max}(E_\infty - E_0) \times \frac{2\sqrt{E_\infty E_0} + (E_\infty + E_0)\sqrt{1+\eta_{\max}^2}}{\eta_{\max}^2(E_\infty + E_0)^2 + (E_\infty - E_0)^2}\right]$$

Example 2.6 Plot the storage modulus and the loss factor as predicted by a FD model that best fits the experimental behavior of the *VEM* Dyad 606 (Soundcoat, Deer Park, NY) at 37.8°C (100°F). Compare the predictions with those of a Poynting–Thomson model.

Solution

The storage modulus and the loss factor of the FD and Poynting–Thomson VEM models are plotted versus the frequency ω as shown in Figure 2.18. The plots are obtained for

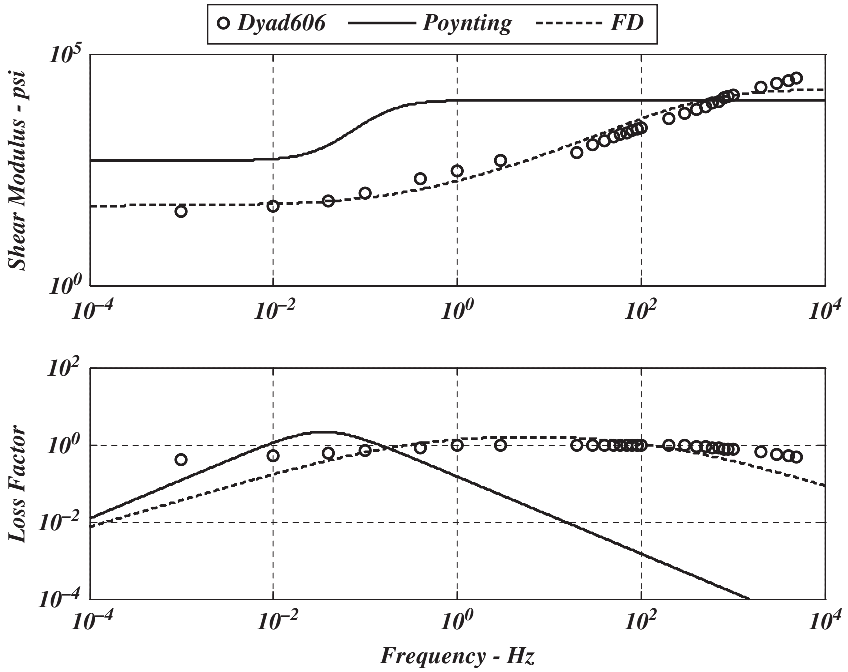

Figure 2.18 Storage modulus and loss factor of a fractional derivative and Poynting–Thomson models.

the Poynting–Thomson model with $\alpha = 1$, $\beta = 20$, $\lambda = 3$, and $E_s = 500\,psi$ while the FD model is given by:

$$\sigma = \frac{52.5 + 18000(0.004s)^{0.7}}{1 + (0.004s)^{0.7}}\varepsilon$$

The figure indicates clearly that the four-parameter FD model adequately replicates the physical behavior of Dyad 606 unlike the linear Poynting–Thomson model.

2.6.3 Other Common Fractional Derivative Models

In this section, some of the commonly used FD models are introduced. The main characteristics of these models are presented in the frequency ω domain as indicated in Table 2.12. These models vary in complexity by increasing the number of the included parameters from three (E_∞, Δ, τ) as in the Debye model to five parameters (E_∞, Δ, τ, α, and β) as in the Havriliak–Negami model (Pritz 2003, Ciambella et al. 2011).

Example 2.7 Determine the time response of the following spring-mass system, shown in Figure 2.19, which is damped by a FD damper of the order α:

$$m\ddot{x} + c\tau^\alpha D^\alpha x + kx = f$$

Assume that $m = 1$ kg, $k = 1\ \mathrm{N\,m^{-1}}$, $\tau = 1$ s, $f = 1$ N, and $\alpha = 0.75$. Assume also that $x(0) = 0$ and $\dot{x}(0) = 0$. Use the *Grunwald–Letnikov* (*G–L*) definition of FDs described in Appendix 2.B.5.

Table 2.12 Frequency domain characteristics of fractional derivative viscoelastic models.

Model	***E**(*ω*)**	**Parameters**
Debye	$E^{*} = E_{\infty}\left[1 + \dfrac{\Delta}{1+(i\omega\tau)}\right]^{a}$	3
Cole–Cole[b]	$E^{*} = E_{\infty}\left[1 + \dfrac{\Delta}{1+(i\omega\tau)^{\alpha}}\right]$	4
Cole–Davidson	$E^{*} = E_{\infty}\left[1 + \dfrac{\Delta}{[1+(i\omega\tau)]^{\beta}}\right]$	4
Havriliak–Negami	$E^{*} = E_{\infty}\left[1 + \dfrac{\Delta}{[1+(i\omega\tau)^{\alpha}]^{\beta}}\right]$	5

[a] where $\Delta = (E_0 - E_{\infty})/E_{\infty}$ = relaxation strength, = relaxed elastic modulus, = unrelaxed elastic modulus.
[b] Friedrich and Braun (1992), Pritz (2003), and Ciambella et al. (2011).

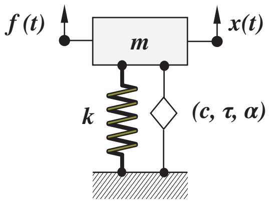

Figure 2.19 A spring-mass system with a fractional derivative damper.

Solution

According to the set parameters, the system equation reduces to:

$$\ddot{x} + D^{0.75}x + x = 1$$

or

$$\ddot{x} = -D^{0.75}x - x + 1$$

where,

$$D^{0.75}x = \lim_{N\to\infty}\left[\left(\frac{t}{N}\right)^{-0.75}\sum_{j=0}^{N-1} A_{j+1}\; f(t - jt/N)\right]$$

where A_{j+1} = Grunwald coefficients.

Figure 2.20a,b displays the Grunwald coefficients and the time response of the spring-mass system with a FD damper, respectively. It is evident, from Figure 2.20a, that the Grunwald coefficients vanish as the number of terms included in the summation of Eq. (2B.14) increases. This demonstrates clearly the “fading memory” characteristics of FDs. Figure 2.20b indicates that the system reaches, with an error of 3.14%, the desired reference command after 15 s.

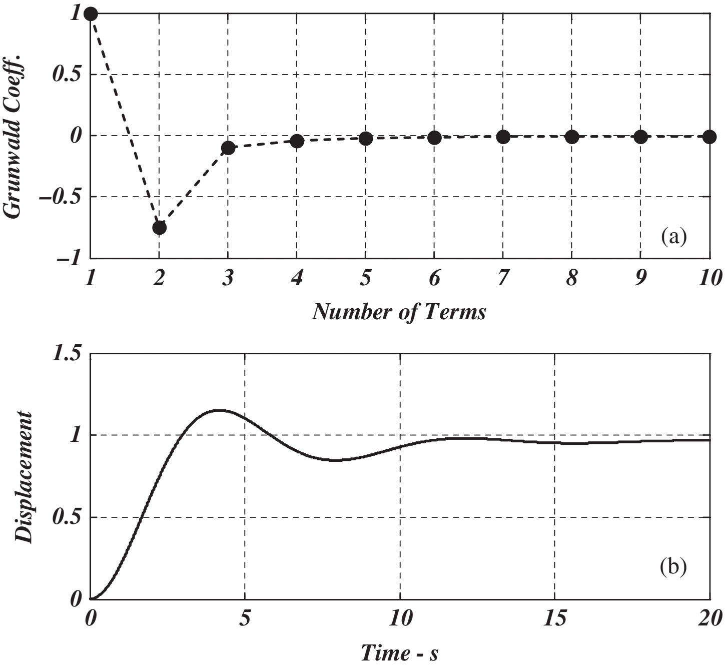

Figure 2.20 Time response of a spring-mass system with a fractional derivative damper.

Note that the approach adopted in Example 2.7 establishes the basis for time domain analysis of finite element models of structures treated with VEMs that are described by FD models.

2.7 Viscoelastic Versus Other Types of Damping Mechanisms

In this section, four important damping mechanisms are presented, including: viscous, hysteretic, structural, and friction damping in order to distinguish, compare, and relate their characteristics to those of viscoelastic damping materials.

Tables 2.13 and 2.14 summarize the main characteristics of these four damping mechanisms. Table 2.13 presents the physical representation of each mechanism, its mathematical model, force-displacement characteristics, and a typical time response behavior.

The energy dissipated per cycle by the different damping forces is calculated as follows:

$$D_i = 4\int_0^{\pi/2\omega} F_d \dot{x}\, dt \tag{2.66}$$

where F_d denotes the damping force as listed in the third column of Table 2.13.

The equivalent viscous damping coefficient, for any damping mechanism, is obtained by equating the energy dissipated by the ith mechanism to that of the viscous damping

Table 2.13 Characteristics of viscous, hysteretic, structural, and friction damping.

Damping mechanism	Physical representation	Model	Force – displacement	Time response
Viscous[a,b]	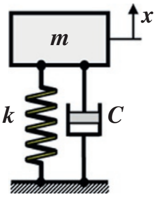	$F_d = c\dot{x}$	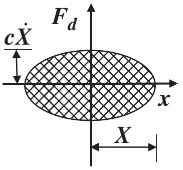	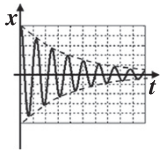
Hysteretic[a,b]	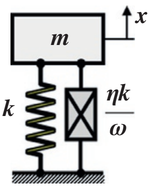	$F_d = \frac{\eta k}{\omega}\dot{x}$	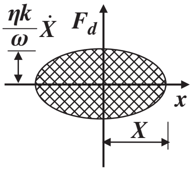	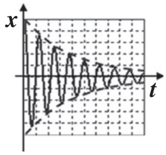
Structural[c,d]	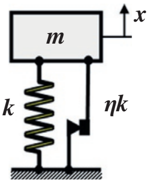	$F_d = \eta k\lvert x\rvert\,\mathrm{sgn}(\dot{x})$	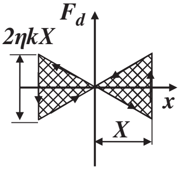	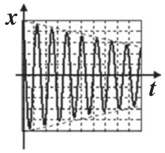
Friction[a,b]	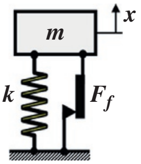	$F_d = F_f\,\mathrm{sgn}(\dot{x})$	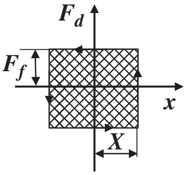	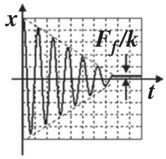

[a] Beards (1996).
[b] Rao (2010).
[c] Muravskii (2004).
[d] Gremaud (1987).

Table 2.14 Energy dissipation and damping ratios of viscous, hysteretic, structural, and friction damping.

Damping mechanism	Energy dissipation	Equivalent damping coefficient	Equivalent damping ratio
Viscous	$D_v = \pi c\omega X^2$	$c_v = c$	$\zeta_v = c/2\sqrt{km}$
Hysteretic	$D_H = \pi k\eta X^2$	$c_H = \dfrac{k\eta}{\omega}$	$\zeta_H = \dfrac{\eta}{2}$
Structural	$D_S = 2k\eta X^2$	$c_S = \dfrac{2k\eta}{\pi\omega}$	$\zeta_S = \dfrac{\eta}{\pi}$
Friction	$D_F = 4F_fX$	$c_F = \dfrac{4F_f}{\pi\omega X}$	$\zeta_F = \dfrac{2}{\pi}\left(\dfrac{F_f}{kX}\right)$
Viscoelastic	$D_{VEM} = \pi k\eta X^2$	$c_{VEM} = \dfrac{k\eta}{\omega}$	$\zeta_{VEM} = \dfrac{\eta}{2}$

mechanism D_v. Hence, the equivalent damping ratio of the ith mechanism is calculated as follows:

$$\zeta_i = c_i/2\sqrt{km} \tag{2.67}$$

Equation (2.67) assumes that $\zeta_i = c_i/c_c$ where $c_c = 2\sqrt{km}$ is the critical damping coefficient for a single degree of freedom vibrating system.

Table 2.14 summarizes the energy dissipated per cycle, the equivalent viscous damping coefficients, and equivalent damping ratios of the different mechanisms in comparison with the corresponding values for viscoelastic materials.

2.8 Summary

This chapter has presented the classical models of VEMs. The merits and limitations of these models have been discussed both in the time and frequency domains. The energy dissipation characteristics of the VEMs have been presented with particular emphasis on the use of the unifying concept of the complex modulus. A brief description of the FD models has also been outlined to emphasize their utility and compactness. Measurement methods of the complex modulus of the VEMs will be presented in the next chapter, and extension of the classical models to more practical models that can be easily incorporated in the formulation of finite element method will be presented in Chapters 4–6.

References

Bagley, R.L. and Torvik, P.J. (1983). Fractional calculus-a different approach to the analysis of viscoelastically damped structures. *AIAA Journal* 21: 741–749.

Beards, C. (1996). *Structural Vibration: Analysis and Damping*. London: Arnold.

Christensen, R.M. (1982). *Theory of Viscoelasticity: An Introduction*, 2nde. New York: Academic Press Inc.

Ciambella J., Paolone A., Vidoli S., "Dynamic Behavior of Viscoelastic Solids at Low Frequency: Fractional vs Exponential Relaxation", 1–5. In Proceedings XX Congresso dell'Associazione Italiana di Meccanica Teorica e Applicata, Bologna 12–15 September 2011; F. Ubertini, *E. Viola*, S. de Miranda and G. Castellazzi (Eds.), ISBN 978-88-906340-1-7, 2011.

Flugge, W. (1967). *Viscoelasticity*. Waltham, MA: Blaisdell Publishing Company.

Friedrich, C. and Braun, H. (1992). Generalized Cole–Cole behavior and its rheological relevance. *Rheologica Acta* 31 (4): 309–322.

Galucio, A.C., Deü, J.-F., Mengué, S., and Dubois, F. (2006). An adaptation of the gear scheme for fractional derivatives. *Computer Methods in Applied Mechanics and Engineering* 195 (44–47): 6073–6085.

Golla, D.F. and Hughes, P.C. (1985). Dynamics of viscolelastic structures – a time domain finite element formulation. *ASME Journal of Applied Mechanics* 52: 897–906.

Gremaud G., "The Hysteretic Damping Mechanisms Related to Dislocation Motion", *Journal de Physique, Colloque C8*, Supplement au N012, Tome 48, December 1987.

Haddad, Y.M. (1995). *Viscoelasticity of Engineering Materials*. New York: Chapman & Hall.

Heymans, N. (1996). Hierarchical models for viscoelasticity: dynamic behaviour in the linear range. *Rheologica Acta* 35 (5): 508–519.

Iwan, W.D. (1964). An electric analog for systems containing Coulomb damping. *Experimental Mechanics* 4 (8): 232–236.

Lakes, R. (1999). *Viscoelastic Solids*. Boca Raton, FL: CRC Press.

Lakes, R. (2009). *Viscoelastic Materials*. Cambridge, UK: Cambridge University Press.

Lesieutre, G.A., Bianchini, E., and Maiani, A. (1996). Finite element modeling of one-dimensional viscoelastic structures using anelastic displacement fields. *Journal of Guidance, Control, and Dynamics* 19 (3): 520–527.

Lesieutre, G.A. and Mingori, D.L. (1990). Finite element modeling of frequency-dependent material damping using augmenting thermodynamic fields. *Journal of Guidance, Control, and Dynamics* 13 (6): 1040–1050.

Muravskii, G.B. (2004). On frequency independent damping. *Journal of Sound and Vibration* 274: 653–668.

Nashif, A., Jones, D., and Henderson, J. (1985). *Vibration Damping*. New York: Wiley.

Nise, N.S. (2015). *Control Systems Engineering, 7th Edn*. Hoboken, NJ: Wiley.

Oldham, K.B. and Spanier, J. (1974). *An Introduction to the Fractional Calculus and Fractional Differential Equations*. New York: Wiley.

Padovan, J. (1987). Computational algorithms for FE formulations involving fractional operators. *Computational Mechanics* 2: 271–287.

Podlubny, I. (1999). *Fractional Differential Equations*. San Diego, California: Academic Press.

Pritz, T. (2003). Five-parameter fractional derivative model for polymeric damping materials. *Journal of Sound and Vibration* 265: 935–952.

Sun, C. and Lu, Y.P. (1995). *Vibration Damping of Structural Elements*. Englewood Cliffs, NJ: Prentice Hall.

Rao, S.S. (2010). *Mechanical Vibrations*, 5the. New Jersey: Prentice Hall.

Vondřejc, J. (2009). *Constitutive models of linear viscoelasticity using Laplace transform*. Czech Republic, Prague: Department of Mechanics, Faculty of Civil Engineering, Czech Technical University.

Zener, C.M. (1948). *Elasticity and Anelasticity of Metals*. Chicago: University of Chicago Press.

2.A Initial and Final Value Theorems

The initial and final values of a function $x(t)$ are given by the following theorems (Nise 2015):

- *Initial value theorem:* $x(0) = \lim_{t \to 0} x(t) = \lim_{s \to \infty} sX(s)$
- *Final value theorem:* $x(\infty) = \lim_{t \to \infty} x(t) = \lim_{s \to 0} sX(s)$

Proof

From the definition of the Laplace transform **L**:

$$\mathbf{L}\left[\frac{d}{dt}x(t)\right] = \int_0^\infty \left[\frac{d}{dt}x(t)\right] e^{-st} dt = sX(s) - x(0)$$